DOCUMENTING HYDROMETEOR LAYER OCCURRENCE WITHIN INTERNATIONAL SATELLITE CLOUD CLIMATOLOTY PROJECT-DEFINED CLOUD CLASSIFICATIONS USING CLOUDSAT AND CALIPSO

by

Forrest Wrenn

A thesis submitted to the faculty of
The University of Utah
in partial fulfillment of the requirements for the degree of

Master of Science

Department of Atmospheric Sciences

The University of Utah

May 2012

The University of Utah Graduate School

STATEMENT OF THESIS APPROVAL

The thesis of **Forrest Wrenn**

has been approved by the following supervisory committee members:

Gerald G. Mace	, Chair	**01/26/2012** Date Approved
Courtnay Strong	, Member	**01/26/2012** Date Approved
Steven K. Krueger	, Member	**01/26/2012** Date Approved

and by **Kevin Perry** , Chair of the Department of **Atmospheric Sciences**

and by Charles A. Wight, Dean of The Graduate School.

ABSTRACT

The multi-decadal and global International Satellite Cloud Climatology Project (hereafter ISCCP) dataset has proven invaluable to the modeling community. ISCCP provides information only on the effective radiative top of cloud layers in a vertical column and the column-integrated optical depth. The effective radiative cloud top has been used to characterize cloudy pixels in terms of certain morphological types even though this is known to be inaccurate. In the presence of multiple clouds layers, such as cirrus over boundary layer clouds, the effective radiative cloud top may have little to do with the geometric distribution of hydrometeor layers. This ambiguity in the presence of multiple cloud layers leads to possible misinterpretations of ISCCP statistics when cast into the traditional cloud top pressure-optical depth classifications. CloudSat and CALIPSO provide detailed information regarding the vertical structure of clouds layers but on a much coarser temporal and spatial grid. Therefore, we use the detailed information from CloudSat and CALIPSO to document the actual distribution of cloud layers within the ISCCP cloud classifications. Cloud properties provided from CloudSat and CALIPSO combined with atmospheric state data from ECMWF and column optical depth from MODIS are input into an ISCCP simulator code to provide ISCCP-like cloud top pressures and the active remote sensing data are used to explore the vertical structure of cloud and precipitation layers within the standard nine ISCCP cloud top pressure-optical depth classifications. We will show that ISCCP-defined "types" defy a simple

interpretation and are often ambiguous within a region and entirely nonunique between regions calling into question recent results that attempt to use ISCCP global statistics to evaluate model results.

TABLE OF CONTENTS

CHAPTER 1

INTRODUCTION

Uncertainties in the representation of cloud feedbacks in global climate models (GCMs) have been consistently identified as the primary source of uncertainty in prediction of anthropogenic climate change (Dufresne and Bony, 2008). Dufresne and Bony 2008 are able to show, under a doubling of CO_2 scenario, that clouds account for nearly one-third of the feedbacks responsible for the temperature response in climate models. Moreover, Dufresne and Bony (2008) showed that clouds contribute, by far, the most intermodel feedback variability among the models used in the study; it was responsible for 70 percent of the standard deviation of the temperature spread (Dufresne and Bony 2008). Although this study treated the feedback processes as linear, it still illustrates the importance of clouds and the effect by clouds on the intermodel differences. Additionally, the responses of convective and boundary layer clouds both contribute to the spread of global cloud feedbacks in GCMs, with a dominant role of intermodel differences in the response of low-level clouds (Bony 2006). Soden and Vecchi (2011) found that the intermodel spread arises principally from differences in the shortwave feedback, which ranges from modestly negative to strongly positive. Additionally Soden and Vecchi (2011) found that high clouds provide a relatively consistent and weakly positive feedback in these models, whereas low cloud feedback is variable in both magnitude and sign. The last 30 years we have been relying on passive

radiometer retrievals that did not resolve cloud vertical structure (this latter had to be derived from field program radar measurements or radiosonde-based retrievals), and that mainly provided column-integrated or cloud-top retrieval products (Bony 2006). Toward an improvement this study attempts to apply active remote sensing to explore this uncertainty. The A-Train constellation of satellites provide real observational advances in cloud property retrievals: new observations from active space-borne radar and lidar, in synergy with other instruments, will provide vertical profiles of multilayer cloud amount, cloud condensate, cloud phase properties, and microphysical size distributions and precipitation (Bony 2006). The main focus of this study is an investigation of cloud macrophysical properties.

A brief excursus is worthwhile to investigate the differences between cloud forcing and cloud feedbacks. First we have a look at the equation (Bony 2006) describing cloud forcing, then we move to examples. CRF represents the cloud radiative forcing and R and R_{clear} represent net radiation in all-sky and clear-sky, respectively. CRF is the top of atmosphere (TOA) radiative forcing measured, or calculated, as the difference between cloudy and clear conditions.

$$CRF = R - R_{clear} \tag{1.1}$$

We start with the simple example of low-lying stratocumulus cloud forcing and move to more complex ideas of cloud feedback. Stratocumulus clouds are lower in the atmosphere and generally are thick. Hence, the cloud forcing generally associated with stratocumulus clouds is negative forcing for shortwave radiation because of their high

optical depth, recognizing that albedo is correlated with visible optical depth. With respect to longwave radiation, low-lying clouds have small positive forcing. The small radiative effect in the longwave range is because low-lying clouds do not produce a drastic temperature difference between the cloud tops and the surface of the earth, citing that the radiative effect is driven by the Stefan-Boltzmann equation. It is worthwhile to note that the temperature difference between the cloud top and the surface of the earth depends greatly on the atmospheric constituents, i.e., concentrations of CO_2, and water vapor make the clear-sky more optically opaque and reduce the clear-sky versus cloudy difference. Cirrus clouds on the other hand tend to be thinner and are much higher in the atmosphere. Thus, they are considered to have a slight to negative shortwave radiative effect, as they have low visible optical depth. Their longwave radiative forcing tends to be strongly positive. This is because they are high in the atmosphere and produce a strong gradient between their cloud top temperature and the temperature at the surface of the earth. It is worthwhile to note, as with low clouds, that the longwave radiation can be affected by the often-tenuous nature of cirrus clouds that do not have an emissivity of unity. That is, the top of atmosphere (TOA) radiative effect may have contributions from lower layers as well as from the cooler cloud top of the cirrus clouds.

Cloud feedback is the response clouds have on the climate and vice versa. Clouds not only affect the climate through radiative forcing, but are also subject to the changes within the climate itself. Through this reasoning they are considered a form of internal forcing. The idea of positive or negative feedbacks with respect to different cloud types can be an abstract idea. Cloud feedbacks must be measured in a model, as the change from a present state to some future point via some imposed forcing. Stephens (2005)

defines feedback by the following equation (1.1) that represents the difference in radiative forcing due to a certain feature (i.e. clouds) between two equilibrium states divided by the change in surface temperature between those states.

$$f_i = \frac{1}{\lambda} \sum_{j=1}^{n} \frac{\partial R_{TOA}}{\partial X_j} \frac{dX_j}{dT} \tag{1.2}$$

In the equation, f_i is the feedback parameter, λ is the climate sensitivity, R is the radiative response at the top of atmosphere, X represents whatever process in the atmosphere is causing the feedback, and T represents the change in temperature, or for our purposes the surface temperature. For our purposes, X would represent the cloud radiative effect. Staying with our simple example of low-level clouds, it has been shown that they cause negative forcing. Now consider a climate model that has an induced warming due to increasing CO_2 concentrations. Furthermore, for the sake of this example, it is easier to think of this feedback for a particular region or locally. One particular region that has copious amounts of stratocumulus decks that have a negative radiative forcing are the eastern coasts of ocean basins, particularly the Pacific. Under certain circumstances these clouds can have a positive feedback, i.e., in a changing climate there may be less of this particular cloud type in a region. The reduced amount of low-level clouds in this region would represent a positive cloud feedback because there are less of these particular clouds with their negative forcing. The fewer clouds would mean that there is less negative radiative forcing from this region and could facilitate more warming. The forcing predicted by climate models is sensitive to how the models

treat clouds in a warming climate. If we were to consider the opposite effect, i.e., a warming climate from imposed increases in CO_2 producing more low clouds, then we would observe a negative feedback as the increased amount of cloud cover would force the warming climate back toward equilibrium.

To use another example we could also examine what sort of climate feedback we would expect from high clouds. We stated earlier that cirrus clouds, or high clouds, impose a positive forcing cloud forcing. So as before if we have a warming climate through the imposition of increase CO_2 concentrations, it would depend on how the models treat the occurrence of cirrus clouds. For example, if the warming climate produced less cirrus clouds, then the positive forcing associated with cirrus would be counteracted by their less frequent occurrence thus producing a negative feedback. To consider what happens under the contrary circumstances, if the warming climate produces more cirrus, then that would constitute a positive forcing and exacerbate the move of the climate away from its original stasis. The next section explains how models or GCMs treat clouds and whether this change in the frequency of occurrence, or their properties would affect the climate system.

Soden and Vecchi (2011) investigated these different cloud types, their radiative forcing, and feedbacks. The type of feedback is strongly related to the production of more or less of certain cloud types under a warming climate. It is shown, for example, that the stratocumulus regimes on the eastern margins of ocean basins have a positive cloud feedback that can be seen linked to reduced liquid and ice water paths (Soden and Vecchi 2011). As mentioned before, the feedback being considered varies by cloud type and by the wavelength. However the models tend to find the total cloud feedback to be

neutral to strongly positive (Soden and Vecchi 2011). The range in the overall feedback can be decomposed and the feedback can be analyzed to deduce which cloud types create the largest uncertainty. Indeed, Soden and Vecchi (2011) find that low clouds create the most intermodel uncertainty while high clouds change similarly among the models. Understanding the source of the cloud feedback uncertainty and ultimately reducing this uncertainty requires measurements of the properties of clouds in the earth's atmosphere. Case studies and high-resolution modeling are emerging as a viable approach to understanding the processes that must be parameterized (Iga et al., 2011). However, the use of global datasets describing cloud occurrence and macroscopic properties has always been necessary to validate the impact of new parameterizations on GCM performance and to asses the skill of GCMs to faithfully represent the Earth's climate since global measurements from satellites became available (e.g., Zhang et al, 2005). This is especially necessary because of the inherent disconnect between GCMs and the inability of them to explicitly produce clouds. Even with the advent of the necessary computing power to bridge the gap between the resolutions of say GCMs and smaller-scale cloud resolving models (CRMs), the need for global data sets describing cloud micro and macrophysical processes is clear.

The International Satellite Cloud Climatology Project (ISCCP) data (Rossow and Schiffer, 1999) uses weather satellite observations and global retrievals of thermodynamic state to derive cloud occurrence, the column optical depth, and the effective cloud top pressure. This data set is global, spans nearly 30 years, and has emerged as a baseline against which our understanding of cloudiness in the earth's atmosphere is based (Rossow and Zhang, 1995; Hartmann et al., 2001; Jakob and

Tselioudis, 2003) and a standard against which models are assessed (Zhang et al., 2005, Williams and Tselioudis, 2007).

Because the ISCCP algorithms use weather satellite information that is typically limited to a single visible and a single thermal infrared measurement, the precision of the ISCCP algorithms to characterize the properties of clouds is inherently limited. Fundamentally, the visible reflectance is used to derive the column optical depth (τ) and the thermal infrared radiance to derive the effective cloud top pressure (P_{top}) after making simplifying assumptions. These assumptions run the gamut of calibration among radiometers of different ages to the actual detection of the two variables of concern for this study. The most obvious assumption is that clouds are assumed to be single layer. Subsequent data products provided by ISCCP have attempted to account for multiple layers. Another assumption that concerns the derivation for the infrared radiance is that accurate temperature profiles can be derived from a space-borne temperature profiler. The cloud top temperature is computed in a radiative transfer model and used to constrain the observed radiances and cloud top temperature (Rossow and Schiffer, 1999). With respect to the visible reflectance that is used to calculate τ, assumptions are made about scattering of ice or water clouds.

That temperature is then matched to the corresponding temperature in the atmospheric profile; the profile is derived from the Television Infrared Observation Satellite (TIROS) Operational Vertical Sounder (TOVS) product produced by NOAA NESDIS (Rossow and Schiffer 1999). There are inherent sources of error that must be addressed when using this method. Assuming a single layer cloud, the errors can be threefold. A discussion of multiple layers is deferred to the next section. The main

sources of error in cloud top temperature are from radiometer calibration, the radiative transfer model treatment of cloud emission and scattering, the treatment of water vapor absorption/emission above the cloud, and errors in the atmospheric temperature-humidity profiles (Rossow and Schiffer 1999). It is worthwhile to note that diffuse cloud tops will bias lower with respect to altitude much like cloud tops in the presence of multiple layers, especially those consisting of thin cirrus over low clouds.

Other passive remote sensors such as MODIS suffer from some of the same limitations. ISCCP takes a liberal approach of assigning as thin cirrus any clouds which are detected but for which an optical depth cannot be determined; this MODIS dataset uses a conservative approach and disregards data for which an optical depth cannot be assigned (Williams and Webb 2008). There can also be discrepancies between these two similar sensors. Another problem for both observational datasets is where several cumulus clouds, with clear-sky between, are contained within a pixel. In these situations, the observations will be biased to indicate clouds that are thinner and more extensive than is actually the case. An estimate of the effect of sub-pixel variability on the shallow cumulus cluster is presented by Williams and Tselioudis (2007). With the exception of this issue with shallow cumulus, studies comparing ISCCP with other observational datasets suggest more uncertainty in P_{top} than τ (e.g., Mace et al. 2006; Wang et al. 1998), particularly in multi-layer cloud situations (Williams and Webb 2008).

The first source of error, radiometer calibration, is accounted for in data processing. The release of the latest ISCCP data products offered improvements to the radiance calibrations to reduce spurious changes in the long-term radiance measurement record provided by ISCCP as well as an improved treatment of the radiative transfer, e.g.,

adding scattering in the infrared (Rossow and Schiffer 1999). The last source of error, treatment of water vapor absorption/emission, is most likely due to the intrinsic difficulty of using a passive remote sensor to compute a temperature profile given the complex weighting functions. Weighting functions must be applied to the temperature sounder. This is because it measures the temperature of different atmospheric constituents based on its mixing ratio throughout an atmospheric column. However each constituent does not emit from a single discrete layer in the atmosphere, but it follows a weighting function to estimate the contribution of a given constituent as a function of height. This is increasingly difficult given the horizontal inhomogeneity of the atmosphere; some constituents are not uniformly mixed as a function of latitude or longitude, e.g., water vapor. For example, values of water vapor throughout the height of the atmospheres are higher in the tropics than at polar latitudes. Lastly, water vapor has a very complex emission spectrum. As such, temperature soundings that are remotely sensed are constrained by a radiative transfer model. This underscores the need to provide a geometric description of certain cloud macro-physical properties, e.g., cloud top pressure. CloudSat can provide this geometric description because it remotely senses the hydrometeor occurrence as a function of height, while conversely, ISCCP cloud be thought to provide a radiative distribution of cloud tops. The cloud tops are considered to be a consequence of the radiative properties because the ISCCP algorithm locates the corresponding cloud top pressure based on the column brightness temperature. Although there are uncertainties with any type of remote sensing instrument, there can be value added through the application of active remote sensors. A discussion of the assumptions and complications of CloudSat and CALIPSO are detailed later.

With respect to the last source of error Hartmann (2001) attempts, using ISCCP, to examine why the combined radiative effect of these cloud regimes produces no large net radiative effect for the tropical regions in the study. Hartmann postulates that the radiative balance is not coincidental, as Kiehl (1994) ascertained, but owes itself to dynamical processes between clear and cloudy areas attempting to maintain stasis. Simulations show that the observed cancellation is a universal feature of tropical climate, yet given the uncertainties in the representation of cloud radiative properties by GCMs and cloud resolving models (CRMs), this may not be a definitive result according to Bony et al. (2006). Therefore, measuring the net radiative effect of clouds becomes dubious if the actual distribution of clouds cannot be accurately described. GCMs that overproduce, or under-produce, certain cloud regimes would not then accurately evaluate the net radiative effect of a scene. Implementation of an accurate description of cloud regimes and their occurrence is vital to ascribe the appropriate radiative effects.

The ISCCP simulator was originally developed by Klein and Jakob (1999) and subsequently utilized for intermodel comparisons of clouds and their radiative effects with the ISCCP data set. The simulator can be broken down into two main components (Klein and Jakob 1999, Mace et al. 2010); the first is the statistical downscaling technique, known as the SubgridCloud Overlap Profile Sampler (SCOPS), and deals with the different grid scales used in GCMs (Klein and Jakob 1999), and the other component, ISCCP Cloud Radiances Using SCOPS (ICARUS), takes the data from the GCM and computes the cloud-top pressure and visible optical depth in a manner that is similar to what ISCCP would produce from satellite measurements. This study, similar to Mace et al. (2010), does not need the downscaling portion of the ISCCP simulator

(SCOPS) as measurements are being used as input and not models with varying grid sizes but only uses the portion that takes input and calculates the cloud top pressure and optical depth (ICARUS). All the information that is needed for the ISCCP simulator is provided by the observations from CloudSat and its other data products. Mace et al. (2010) found that the ISCCP simulator was able to produce accurate radiative brightness temperatures, meaning that it accurately simulates the cloud top pressure similar to what ISCCP would measure. However, Mace et al. (2010) noted that there is some uncertainty with the optical depth calculated from the ISCCP simulator. This study, the ISCCP simulator did not calculate the optical depth, rather it was forced to match the CloudSat column integrated optical depth product 2B-Tau. A detailed description of the data products and process used follow in the methodology section.

Cloud top pressures and optical depths then form the foundation for further analysis. Often joint histograms of P_{top} and τ are produced that describe in a gross sense the statistical characteristics of the clouds in a region and during a time period under consideration. It has been understood from the outset of ISCCP that ambiguities associated with the retrieval of P_{top} and τ preclude their use to simply classify an atmospheric column as one cloud type or another (Rossow and Schiffer, 1991). These ambiguities can also be due to the presence of multiple layers of unknown infrared opacity in a vertical column. For instance, thin cirrus over a boundary layer stratus layer would have an infrared radiance that implies cloud tops in the middle troposphere while the visible reflectance of the stratus would suggest that an optically thick middle tropospheric layer is present. To overcome this ambiguity, it has been common practice to use a coarse histogram of 9 P_{top} -τ bins to describe statistical distributions derived from

ISCCP retrievals, and for ease of understanding, these bins have been given names that suggest certain common cloud types (Rossow and Schiffer, 1999).

Traditionally, assessment of clouds in GCMs has been based on comparing maps or global averages of cloud variables—typically total cloud amount or cloud radiative forcing (CRF; e.g., Cess et al. 1990; Pincus et al. 2008; Gleckler et al. 2008). However a GCM can perform well on such metrics through compensation of errors in the temporal frequency and radiative properties of different cloud types, which may result in an incorrect cloud radiative response under climate change (e.g., Webb et al. 2001; Williams and Webb 2008).

With this in mind, the use of ISCCP climatologies currently takes two forms. The first is the straightforward comparison of model output that are compiled into P_{top}-τ bins with similar ISCCP statistics after the model output has been passed through a simulator code that accounts for the ambiguities noted above (Klein and Jakob, 1999). The simulator was originally developed to bridge the gap between GCM cloud parameterizations, numerical weather models, and observations. Numerical cloud output from GCMs is run through a simulator designed to create data based on the same set of assumptions as ISCCP. There are some potential drawbacks to this method. First and of particular relevance to this study, is that the validation of the model relies on the simulated ISCCP data formed from GCM output being cast into coarse cloud top pressure and optical depth bins that may not accurately describe what is actually contained within those bins.

Zhang et al. (2005) present a recent and very thorough example of the first type of analysis through an intermodel comparison. Zhang et al. (2005) compared 10 model

outputs to satellite data provided by ISCCP D2 data product and CERES. The ISCCP simulator discussed in this study was employed in the model data for comparison purposes. The ISCCP simulator not only minimizes the difference of sampling geometry (between CERES and ISCCP observations) but also allows the comparison of model cloud types with measurements that are stratified into both altitude ranges and optical properties (Zhang et al. 2005). By doing this, they are able to provide a benchmark for measuring the effectiveness of the model to accurately produce cloud occurrences. The drawbacks to using passive sensor cloud macro-physical data are addressed by Zhang et al. (2005) before entering a discussion about the models' efficacy. In addition to the innate constraints of passive remote sensing, Zhang et al. (2005) take a brief excurses to addresses the spatial differences between the two satellite systems used (ISCCP and MODIS aboard Terra). Although it is shown that the most difficult type of cloud to model is high, thin cirrus; Zhang et al. (2005) also assert that satellite measurements from ISCCP and CERES alike are very sensitive to optical depth cutoff values and therefore they may not be correctly ascertaining their occurrence.

Zhang et al. (2005) were able to identify three systematic model biases. The grand mean of the models underestimated low to middle cloud tops with intermediate to thin optical depth. The models significantly overestimated the three optically thick clouds at all cloud tops. The mean model output of cloud occurrence was twice the observational data provided by ISCCP and CERES. The models show a seven-fold difference between themselves with the amount of thin cirrus. The intermodel discrepancy is attributed to the differences in the cloud occurrences and could be due to parameterizations used in the models. They are not able to explicitly ascertain the source

of the discrepancies but postulate that intermodel differences could most likely arise from convection triggers or the planetary boundary layer parameterizations or vertical motion in fractional cloud cover scenarios. These convection triggers and planetary boundary layer issues seem to be common to all of the models no matter how they parameterize their cloud schemes: relative humidity, statistical, or prognostic parameterization. These errors represent two of the three systematic errors addressed by Jakob and Tselioudis (2003); these errors will be addressed later in more detail.

Zhang et al. (2005) were able to show that the models, when compared to ISCCP observations, incorrectly produced the number of cloud occurrences with high clouds and middle clouds the most difficult to accurately produce. In terms of optical thickness the models over estimate thick clouds in comparison to ISCCP observations. In addition to the inability of the models to accurately describe cloud occurrence, there is also a large inter-model variability with respect to the number of high clouds produced from the models, a fourfold difference. Zhang et al. (2005) attribute the difference between the models with the ISCCP simulator and the ISCCP observation to deficiencies in the models. However, Mace et al. (2010) were able to show that these same biases occur when ground-based measurements are used as the input to the ISCCP simulator in lieu of model output. This, according to Mace et al. (2010), calls into question not only the ability of models to correctly represent cloud occurrence but the ISCCP simulator that has been used to validate model output. As mentioned before, Mace et al. (2010) find that the largest source of uncertainty in the ISCCP simulator is optical depth with cloud top pressure being more faithfully representative of what ISCCP would measure when compared to ground based remote sensing.

A second class of analyses takes the ISCCP histograms and passes them through a clustering algorithm to identify cloud regimes that are defined by distributions of cloud types. These analyses add an additional layer of abstraction to the ISCCP P_{top}-τ histograms further muddling the convolution of cloud "types" into regimes of muddled cloud types. Jakob and Tselioudis (2003) pioneered this methodology and several important papers have emerged since then (Williams and Tselioudis, 2007; Williams and Webb, 2008) to critically evaluate the ISCCP-defined regimes against what is predicted by GCMs. They employ the KMEANS cluster method and use four distinct clusters. This method seeks to mine data for clusters, by means of measuring between the data points. In this case a ''data point'' is an individual P_{top}-τ histogram forming a vector comprised of its 42 classes (Jakob and Tselioudis 2003). Each histogram is treated as an independent data point and computes the nearest cluster; the number and clusters are predetermined (Jakob and Tselioudis 2003). By varying the number of clusters used, Jakob and Tselioudis (2003) were able to determine patterns that emerge from the data set. These patterns form the four cloud regimes that are the basis for the cluster analysis in Jakob and Tselioudis (2003). The four cloud regimes that are somewhat arbitrarily assigned based on the P_{top}-τ diagrams are: a shallow cumulus regime, a transparent isolated cirrus regime, a thick cirrus with convection regime, and a deep convection regime (Jakob and Tselioudis 2003).

Jakob and Tselioudis (2003) state that the average cloudiness observed in a given region, rather then consisting of a mixture of random cloud fields, is actually composed of a limited number of distinct cloud regimes, each linked to certain characteristics of the atmosphere. They seek to verify this hypothesis by comparing ISCCP data over the

tropical warm pool (TWP) to data provided by the Atmospheric Radiation Measurement (ARM) sites at Manus and Nauru. They find good agreement between the TWP ISCCP measurements and the ARM measurements at Manus, but not at Nauru. This he attributes to the position of island outside of the tropical warm pool in the west Pacific.

It is unclear what technique is used for the identification of cloud layers or if multiple layers were considered for the information gathered at the ARM sites. It is worthwhile to note that although there is good agreement between data from ISCCP over the tropical warm pool and ground-based active remote sensors, his findings show movement of the relative frequency of occurrence (RFO) between ISCCP and ARM data at Manus. Perfect agreement is also not expected from the ARM data even if radar and lidar are used due to differences between the remote sensors orientation, e.g., upward versus downward orientation.

Be that as it may, the motivation for applying this additional level of abstraction to ISCCP data is that GCM cloud feedback error can be decomposed into three components: an erroneous representation of the cloud regimes, an incorrect distribution of the relative frequency of occurrence (RFO) of the cloud regimes, and an incorrect representation of the radiative effects of an individual cloud regime (Jakob and Tselioudis, 2003). A similar clustering analysis to that of Jakob and Tselioudis (2003) was carried out for intermodel comparison purposes in Williams and Tselioudis (2007). Williams and Tseliouids (2007) used clustering analysis to test the fidelity of GCM output through an evaluation of the change in relative frequency of occurrence and cloud radiative forcing of these certain clusters under a changing climate through increased CO_2. Using this clustering analysis, Williams and Tselioudis (2007) found that a large

proportion of the variance in the global cloud response of the six models considered arises from differences in the radiative response of frontal clouds in the ice-free extra-tropics and from stratocumulus in the tropics. This further emphasizes the uncertainty among climate models in the production of low-level clouds that was found in Bony (2006). Furthermore, most of the global cloud response to climate change arises through changes in the radiative properties of the individual regimes (Williams and Tselioudis 2007). However, Williams and Tselioudis (2007) also notes that there is uncertainty with RFO sensitivity as some cloud types might be over/under-simulated to create the observed near-zero net radiative effect in the models.

Williams and Tselioudis showed that not only do the models fail to produce the frequencies of occurrence of various cloud regimes derived from ISCCP, but the radiative effects of the regimes are substantially different from observations, suggesting that the disparity in cloud feedbacks found in climate change scenarios arise not only from a failure to represent the changes in clouds as the climate warms, but also from a failure to properly represent clouds in the present climate (Mace et al. 2010). Williams and Webb (2008) identify that a potential problem with this particular clustering method is that it requires subjective judgment which, together with the subjective decisions remaining within the clustering procedure to define the number of clusters, make the method difficult to automate and for others to apply (Mace et al. 2010).

This necessitates a closer look at whether the sensitivity is to the radiative response of clouds under climate change, or whether it is within the regime definitions. Williams and Webb (2008) investigate this problem by applying the GCM output directly to the ISCCP-defined cloud regime cloud types. Indeed, the ISCCP data are thought to

be capable of characterizing the first two of these three issues raised by Jakob and Tselioudis (2003). This type of method is utilized in an attempt to remove the subjectivity of the clustering method in regime selection. In spite of this, there is still an additional level of abstraction produced by clustering analysis that potentially hides the ambiguity inherent in the ISCCP results more deeply so some care has been taken in interpretation of the results. Figure 1 of Williams and Webb (2008) is an example of a literal interpretation of the P_{top}-τ histograms to represent actual cloud distributions that are taken to represent very specific dynamical regimes in the atmosphere.

Williams and Webb (2008) use a similar clustering method to that used in Jakob and Tselioudis (2003) with similar results. Instead of using predetermined cloud clusters, they assigned the GCM output to the observed ISCCP clusters, since each GCM could have different possible clusters. This eliminates the subjective nature of the predetermination of the cloud clusters. To test the robustness of this method they compare their clustering method to that of Jakob and Tselioudis (2003) with a great deal of similarity. MODIS data were also compared to ISCCP data between the cloud regimes. The agreement between MODIS and ISCCP is not surprising given that MODIS and ISCCP have similar passive remote sensors and pixel size (Williams and Webb 2008).

In the past, as mentioned earlier, studies describing the macrophysical properties have been limited to values gathered by passive remote sensing. The limitations of such observations are well known and well documented. The findings produced from these are then used in model parameterization of clouds. This is because the coarse spatial and temporal resolution of GCMs is unable to explicitly describe clouds. In addition to these

uses, a particular nomenclature has been assigned to cloud regimes that are produced by ISCCP and by models running the ISCCP simulator. What is not known, however, is whether this nomenclature precludes a quantitative understanding of what cloud macrophysical properties actually occur, e.g., cloud layer occurrence for this study. Our goal with this study is to use active remote sensing data provided by the CloudSat Cloud Profiling Radar (CPR) (Im et al. 2006), and the CALIPSO lidar (Winker et al. 2007), to document the actual vertical distribution of hydrometeor layers within the ISCCP P_{top} -τ histogram space in two large regions of the equatorial Pacific. From such an analysis, we demonstrate which of the ISCCP types present significant ambiguities that preclude a simple interpretation of type from the ISCCP P_{top} -τ histograms and ultimately confuse the interpretation of regimes.

The A-Train combination of Aqua, CloudSat, and CALIPSO provides a unique data set for analyzing the macrophysical characteristics of cloud structures globally, and more specific to the scope of this project, the tropics. The Aqua satellite contains the MODIS instrument that is a passive imager operating at various spectral bands from 0.4 microns to 14.4 microns. MODIS provides the radiance data required for the ISCCP simulator. CloudSat follows by approximately 2 minutes behind Aqua and CALIPSO follows CloudSat by approximately 15 seconds. The formation in which they fly allows for nearly simultaneous measurements by the sensors aboard the different satellites. There is some temporal difference due to the lag of the three satellites as well as spatial difference due to a slightly offset formation to account for sun glint. The temporal difference is thought to be negligible in the absence of strong advection or convective

upward motion. The spatial differencing is assumed to be negligible as well considering the resolution of the satellites.

Zhang et al. (2005) were able to show that models fail to correctly create realistic cloud occurrence statistics and these inaccuracies propagate through an analysis of their effects on the climate system. Climate modelers have created their cloud parameterizations based on cloud types and regimes from the ISCCP naming conventions that do little to describe the actual distribution of clouds tops. What exists here are several layers of errors that start with the inaccurate description of cloud types and occurrences in GCMs to an incomplete analysis of the model outputs by using passive remote sensors. These passive remote sensors do not provide explicit information about the geometric distribution of hydrometeors, but rather an implicit description based on a distribution of cloud radiative effects. The goal of this thesis is to more accurately define cloud occurrence distributions within the ISCCP P_{top}-τ histogram space using the explicit definition of geometric heights provided by active remote sensors.

CHAPTER 2

METHODOLOGY

Our objective in this study is to document the actual distribution of hydrometeor layers within ISCCP generated P_{top}-τ joint histograms. Therefore, we need 1) to simulate ISCCP P_{top} and visible τ along the orbital tracks of the CloudSat and CALIPSO satellites, 2) to determine accurate hydrometeor layer bases and tops along these tracks and 3) to compile these into statistical distributions within the ISCCP-defined bins. To accomplish this we use several CloudSat standard data products collected during calendar year 2007 for regions in the tr4opical East and West Pacific. These regions encompass 20˚x20˚ domains centered about the equator and 98˚W and 158˚E, respectively. Figure 2.1 shows a map of these two regions. The selection of the two areas was not arbitrary; they were selected because differences in sea surface temperature and differences in the large-scale vertical motion on either end of the Walker circulation cause distinctively disparate cloud regimes. Typically, the tropical warm pool in the west is more convectively active while the east experiences more suppressed convection due to cooler SSTs and capping inversions. In spite of this difference we surmise that both regions will show multiple cloud layers, albeit with varying frequencies, and magnitude. This hypothesis was the impetus of this study. The dataset provides orbital passes once daily, each pass containing footprints that are approximately 1km in spatial scale along the CloudSat track. Data

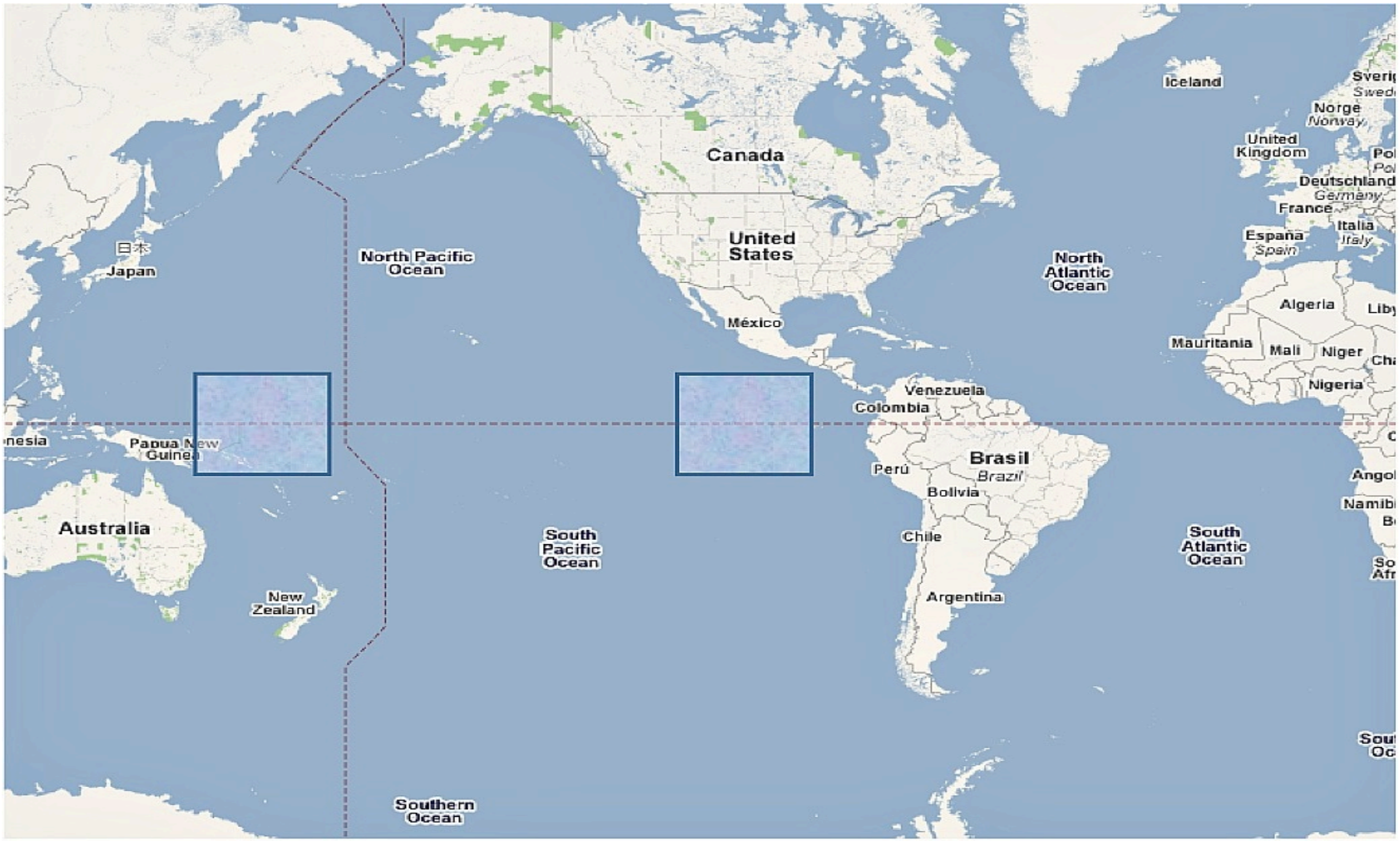

Figure 2.1 A map showing the two regions for this study. The East Pacific region (right) is centered about the equator and 98˚ West. The West Pacific region (left) is located about the equator and 148˚ East.

within the regions of interest were analyzed and ISCCP P_{top}-τ values were simulated as described below. Atmospheric parameters used in simulations and for identification of the pressure profile were provided by along-track ECMWF data in the ECMWF Auxiliary product (ECMWF-AUX) (Partain 2004). It is worthwhile to note that although the ECMWF-AUX product contains a cloud model. However, it is not suspected that it will affect the results too greatly given that the initialization is from a recent time, according to the forecast time and the time of the A-Train over pass, and the cloud processes that would be concerned with feedback processes are on the order of days. Radiances from MODIS data collocated to the CloudSat footprints in the MODIS Auxiliary product (MODIS-AUX), and optical depth (τ) derived from the level 2B-Tau retrievals (Polonsky 2008) were also used; all data were provided by the CloudSat data archive (http://cloudsat.cira.colostate.edu/). Only daytime passes were considered for comparison to ISCCP because visible reflectance is necessary for ISCCP derived optical depth (τ) simulations.

An advantage that we exploit in this study is that the CloudSat CPR and the CALIPSO lidar have the ability to accurately identify the vertical location of hydrometeors in the atmosphere. The CPR also has the distinct ability to map the vertical location of hydrometeor layers even in the presence of optically thick and lightly precipitating higher layers. The CPR has limitations and may not be able to identify tenuous layers such as typically occur near cloud top and because of the reflectance of the ocean surface, layer bases below 1 km cannot be accurately sensed by the radar. The CPR operates at 94GHz and as such is extremely sensitive to the melting layer and precipitation. Partial or full attenuation is possible in profiles that contain more than

moderate liquid precipitation. The lidar aboard CALIPSO is sensitive to small hydrometeors and aerosols and is therefore easily attenuated in the presence of optically thick cloud layers. Even with these limitations, the additional utility provided by combining them is clear and application of active remote sensors can provide a very helpful diagnostic of cloud layers within a profile. For a thorough description of the merged CloudSat-CALIPSO data product known as RL-GEOPROF, see Mace et al. (2009).

Profiles that fall within one of the two regions of the tropics are analyzed. After the bases and tops of hydrometeor layers are identified with RL-GEOPROF, the ECMWF-AUX data are used to identify the pressure profile of the bases and tops. This process is continued for all cloud layers identified within a vertical profile. Because ISCCP is generally insensitive to optically thin cirrus layers that are ubiquitous in the tropical tropopause transition layer (TTL) (Schwartz and Mace, 2010), all cirrus layers with bases above 15km and total optical depth of less than one are excluded from the analysis. The profile is still used even though the high thin layers are removed. A component of the ISCCP simulator known as ICARUS and described in Klein and Jakob (1999) is run for each hydrometeor profile. The ISCCP simulator is designed to take a set of atmospheric variables that are produced by a model and simulate a cloud top pressure (P_{top}) and optical depth (τ) that the ISCCP algorithm would retrieve. This is much the same as how it is used for this study except that some of our "model output" is provided by observations, i.e., MODIS radiances, and optical depth from CloudSat. The ISCCP simulator consists of different components that use atmospheric parameters provided by the data sets described above to ultimately obtain a cloud top pressure.

The first component of the simulator estimates the tropopause level. The temperature profile provided by the ECMWF-AUX is used to locate the temperature inversion at which point the commensurate pressure is also identified. The tropopause locator starts at the highest point in the atmospheric column and works down through the atmosphere to ensure that the low-level temperature inversions are not included. Once the level and temperature of the tropopause are identified, those as well as other information are passed into the temperature simulator. The tropopause level is used as the level where very cold clouds (clouds that have a low infrared radiance) are placed. The temperature simulator also uses clear and cloudy radiances from MODIS-AUX collocated data as inputs. Since MODIS-AUX provides only all-sky radiances, the clear sky radiances had to be parameterized using clear profiles and a nearest neighbor approach. The radiances and optical depth from CloudSat are used to calculate an effective radiative temperature for the profile. Once the radiative temperature of the profile is determined, it is then input into the pressure simulator where the temperature is matched to the ECMWF-AUX temperature profile and its commensurate pressure coordinate. Each CloudSat profile, for instance, would have one cloud top pressure and optical depth, as ISCCP would normally identify within one of its pixels as well as cloud top(s) and base(s) identified by the CloudSat Cloud Profiling Radar. Profiles are then organized in joint histograms according to cloud top height and optical depth corresponding with previous studies in Rossow and Schiffer (1999) and Hartmann (2001).

The first set of joint histograms (Figure 2.2 and 2.3) is arranged into the 42-bin classification first introduced by Rossow and Schiffer (1991). The histograms in

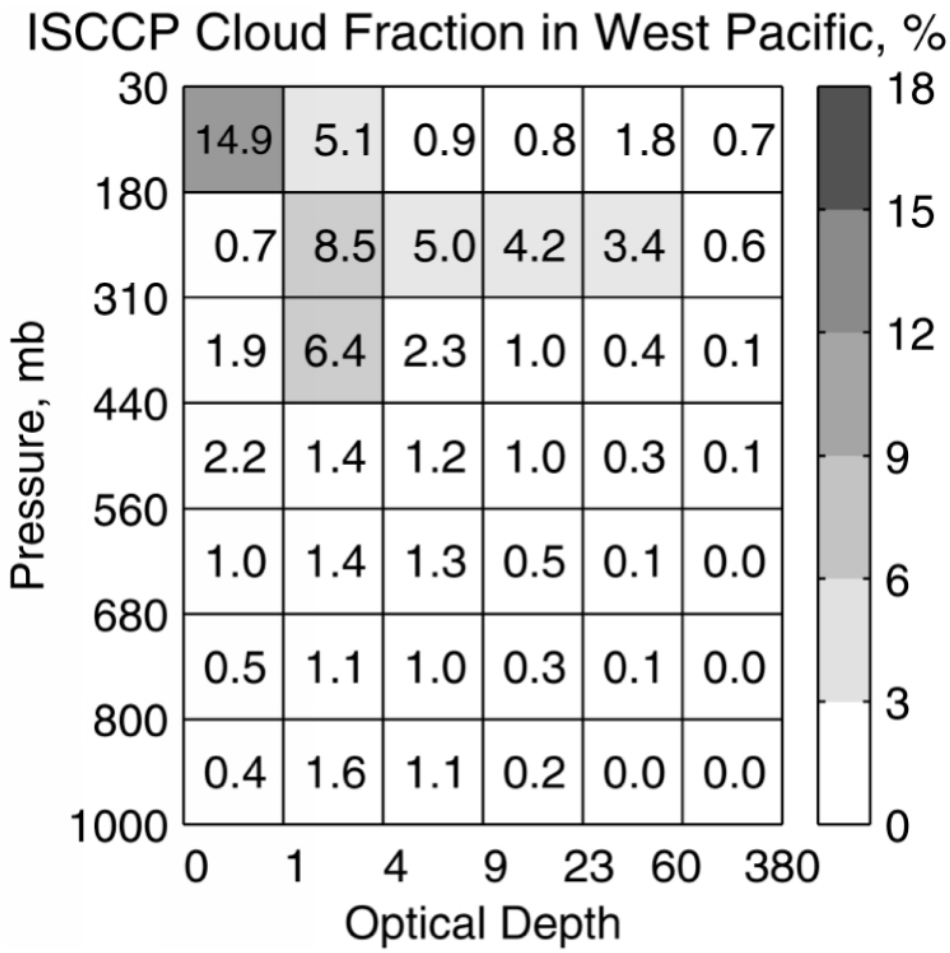

Figure 2.2 Hartmann, D.L., L.A. Moy and Q. Fu, 2001: Tropical Convection and the Energy Balance at the Top of the Atmosphere. *J. of Climate*, **14**, 4495–4511. Figure shows the 42-bin histogram from the West Pacific with frequency plotted as a function of cloud top pressure and optical depth. Darker grays signify higher occurrence. Region encompasses 0˚-15˚N, 120˚E-150˚E. (c)American Meteorological Society. Reprinted with permission.

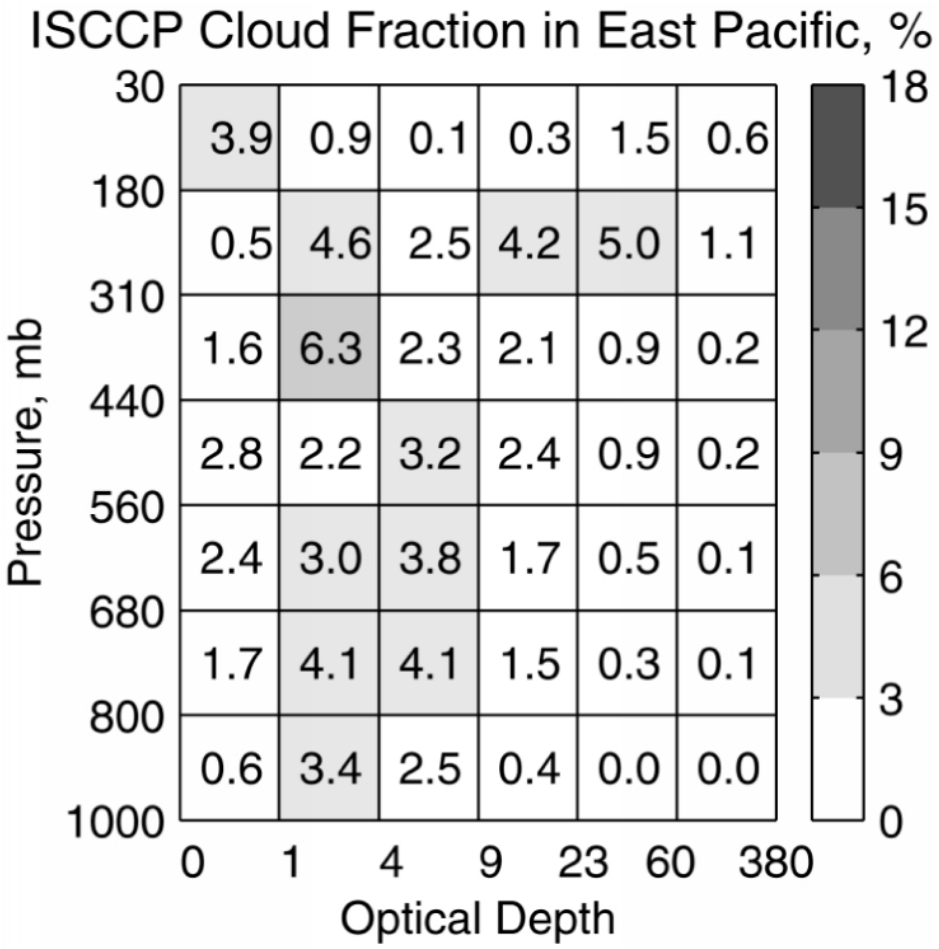

Figure 2.3 Hartmann, D.L., L.A. Moy and Q. Fu, 2001: Tropical Convection and the Energy Balance at the Top of the Atmosphere. *J. of Climate*, **14**, 4495–4511. Figure shows the 42-bin histogram from the East Pacific with frequency plotted as a function of cloud top pressure and optical depth. Darker grays signify higher occurrence. Region encompasses 7.5˚N-15˚N, 100˚W-140˚W. (c)American Meteorological Society. Reprinted with permission.

Hartmann et al. (2001) are ISCCP data from the year 1999 for similar regions in the tropics as were used for this study (West Pacific 0˚-15˚N, 120˚E-150˚E and East Pacific 7.5˚N-15˚N, 100˚W-140˚W). Comparison between these figures and the joint histograms produced for this study for the year 2007 show good agreement; joint histograms produced for this study are shown in the results section. Likewise, the uppermost cloud tops as identified by CloudSat are arranged in the 42-bin method for comparison to ISCCP. The uppermost cloud tops were used in a joint histogram for a purer comparison to ISCCP simulated values, i.e., if ISCCP only records the upper most cloud top pressure from the brightness temperature, then for the sake of this comparison we were interested in the uppermost cloud top pressure based on the cloud geometric height. After validation the CloudSat bases and tops are organized into a coarser nine bin 2-D joint histogram based on the ISCCP cloud top and optical depth identified. An example of the nine-bin histograms and their naming convention can be seen in Figure 2.4. For instance, each cloud top pressure and optical depth bin associated with the nine box joint histogram according to ISCCP contains a distribution of the actual cloud tops and bases based on hydrometeor occurrence from CloudSat. Each vertical profile within a CloudSat pass would have one ISCCP simulated value of cloud top pressure and optical depth. This value would then be matched with one of the coarser nine-bin sections. Each of these profiles that has an ISCCP value would then have cloud tops and bases plotted as a function of height within the bins. Thus the end result is a distribution of cloud layers plotted as a function of height cast into the bins identified by the ISCCP simulator. These coarser bins are associated with cloud regimes that are used in examining cloud parameterizations of models Zhang et al. (2005). In other words, of the nine boxes, the

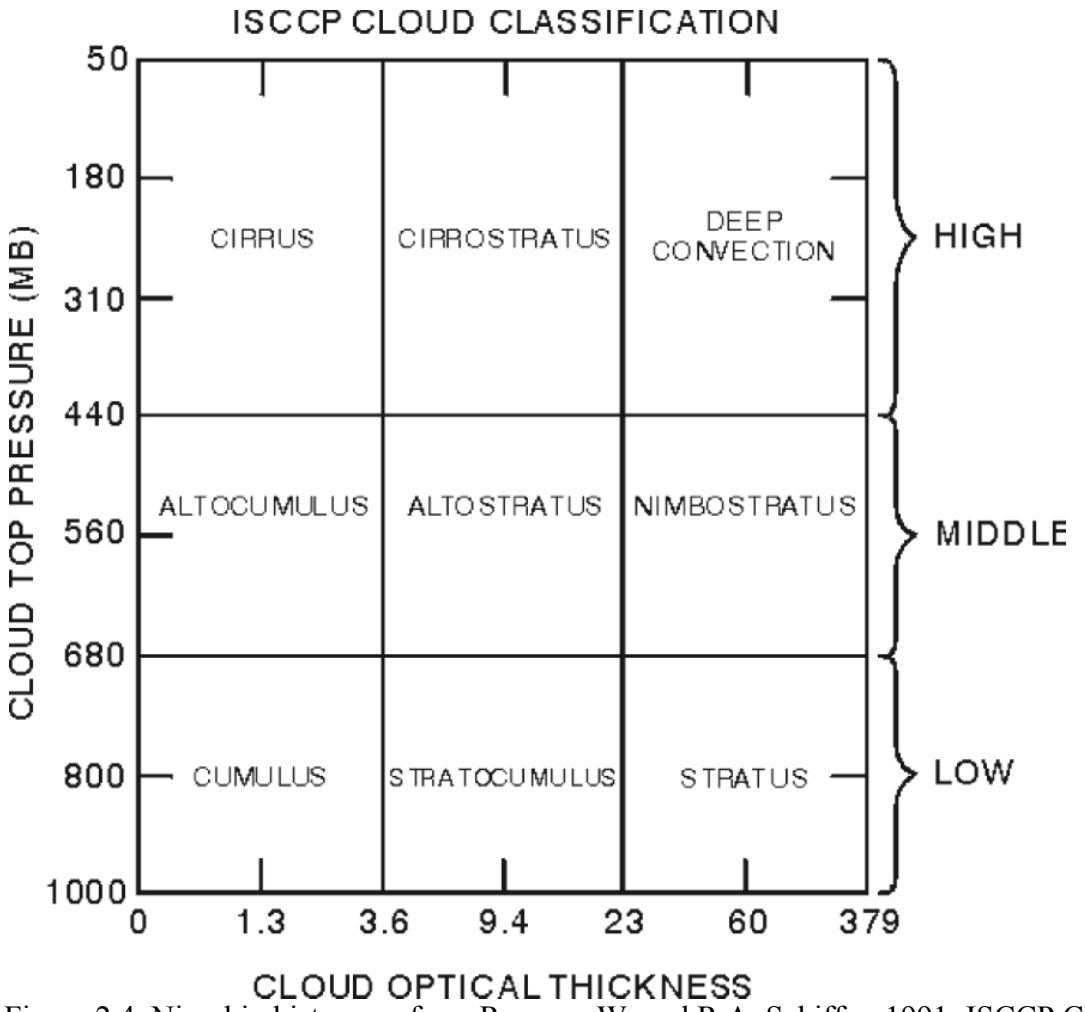

Figure 2.4 Nine-bin histogram from Rossow, W. and R.A. Schiffer, 1991: ISCCP Cloud Data Products. *Bull. Amer. Meteor. Soc.*, **72**, DOI: 10.1175/1520-0477(1991)072<0002:ICDP>2.0.CO;2. Each of the bins in the 42-bin histogram has been combined into coarser bins and assigned names. (c)American Meteorological Society. Reprinted with permission.

one with the lowest cloud top pressure and lowest optical depth would represent cumulus,whereas the lowest cloud top pressure and highest optical depth would represent stratus, and so on.

CHAPTER III

CASE STUDY

Several case studies are analyzed to illustrate the effectiveness of the ISCCP simulator and cloud layer identification algorithm for CloudSat. Case studies are chosen from both the East and West Pacific that illustrate the gamut of cloud types that can occur as well as single and multiple cloud layers. However, the two cases displayed here are both from the East Pacific. Figure 3.1 shows one such case study with a portion of a CloudSat orbit that falls within the East Pacific depicted in the figure. Figure 3.1 shows an overhead view with the 20˚x20˚ region marked by the dark black box. The diagonal lines indicate CloudSat passes. Lines listing from the right to left through the image from bottom to top are ascending (daylight) passes. From bottom to top, the descending passes list from left to right. Ascending passes are synonymous with daytime passes and descending passes (nighttime) were not analyzed in this study. This particular CloudSat orbit passes though the northeast quadrant of the area. Cloud top temperature is plotted over the map as provided by the MODIS instrument aboard Aqua, also in the A-Train. The top panel of Figure 3.2 shows CloudSat and CALIPSO returns from Feb 4 (day of year 35) of 2007 plotted as a function of height and latitude or time. CloudSat and CALIPSO sweep out a curtain over the region so the plot is a 2-D representation with time and height on the abscissa and ordinate, respectively. The figure shows a persistent

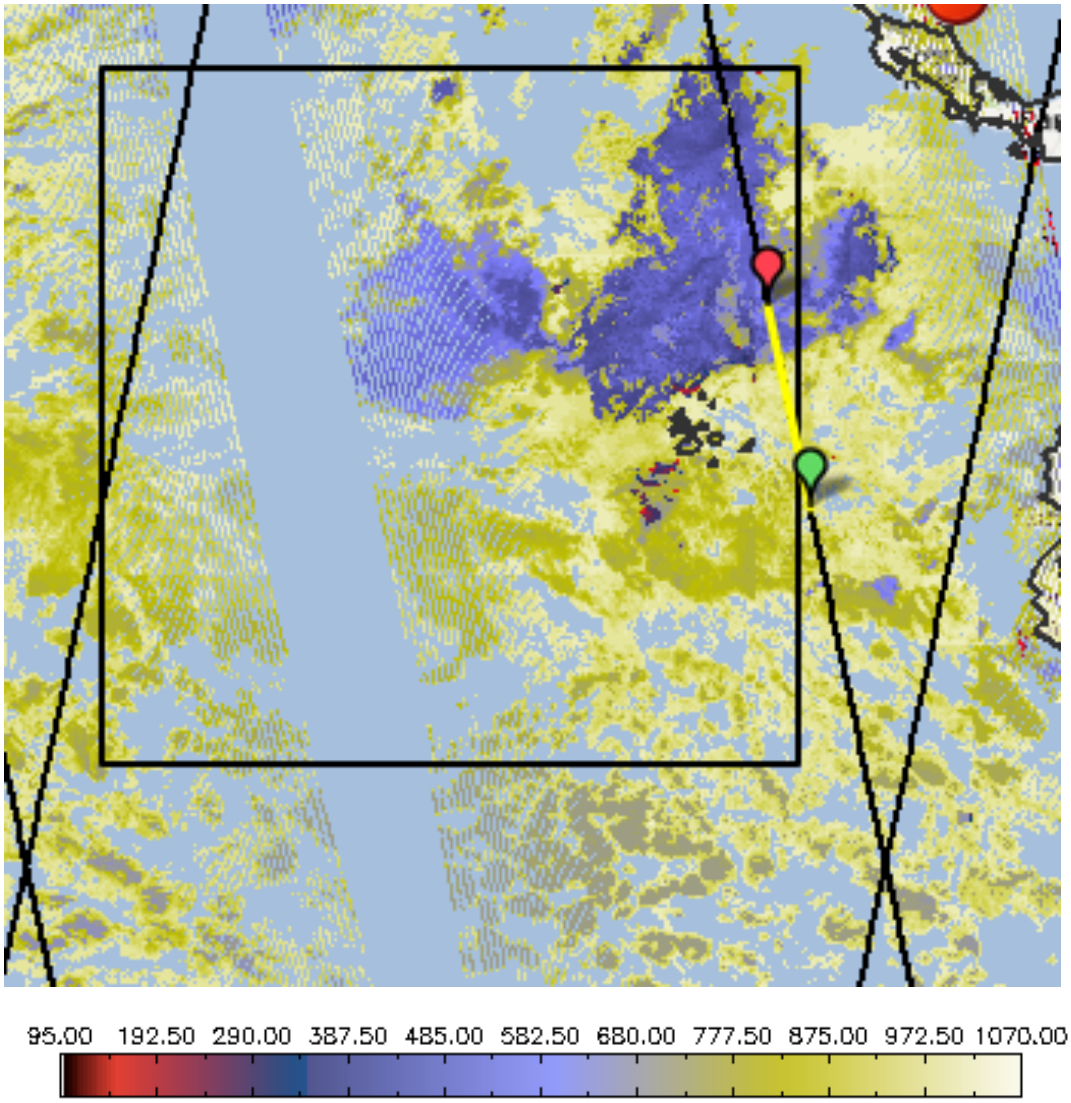

Figure 3.1 Map showing the area in the East Pacific within the black outline of the box. The diagonal lines running through the map are CloudSat passes. Lines that are skewed left with respect to the bottom of the map are ascending passes. Conversely, the other lines represent descending passes. The two pins, green and red, represent a portion of the of the CloudSat pass through the region. Superimposed are cloud top temperatures provided by MODIS aboard Aqua. The pass is from Feb 4 2007.

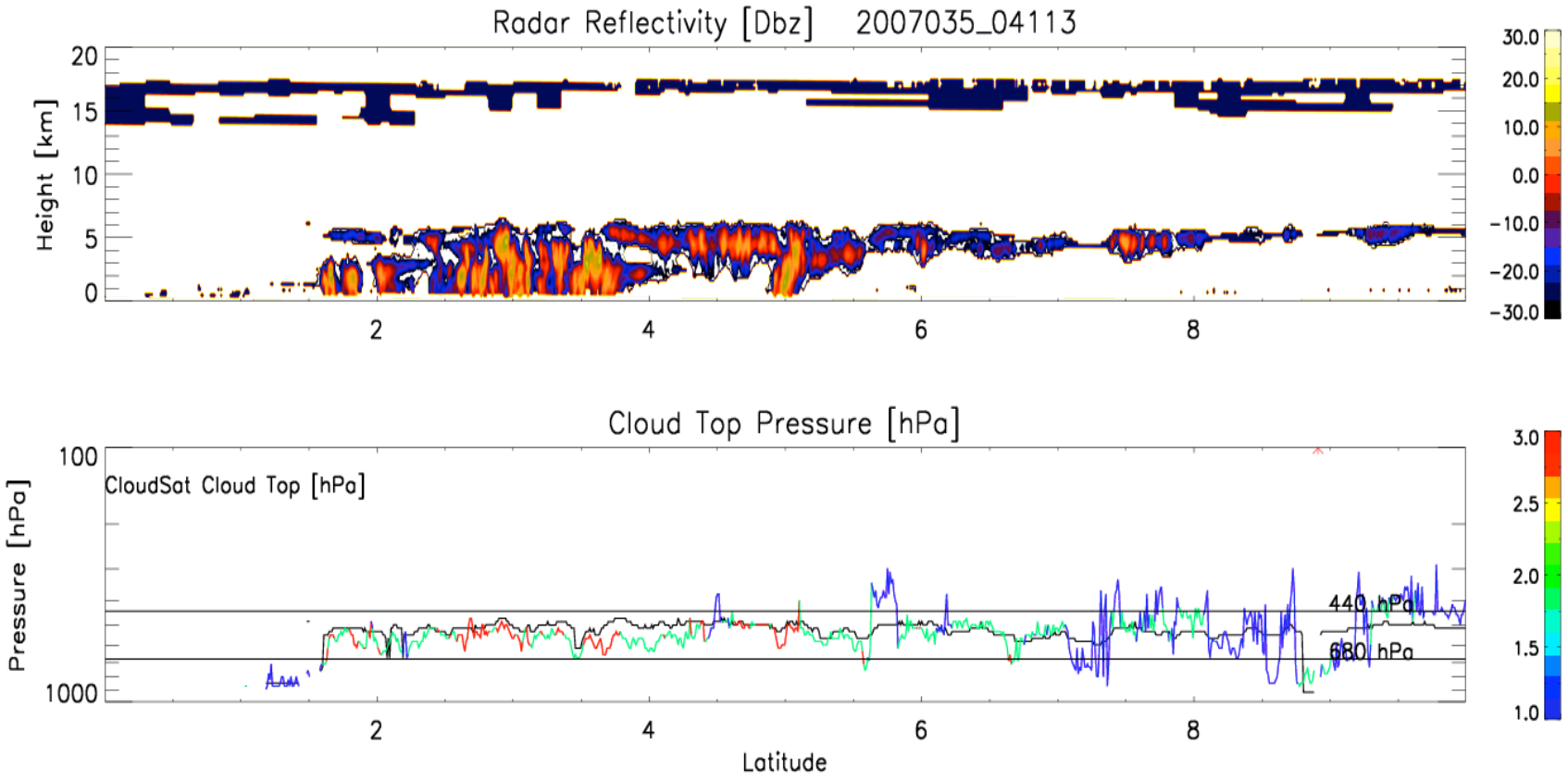

Figure 3.2 R-L GEOPROF profile from 4 February 2007. Top panel displays CloudSat dBZ and CALIPSO plotted as a function of height and latitude (time). Bottom panel displays CloudSat and ISCCP cloud tops plotted as a function of pressure and latitude (time). CloudSat cloud tops are plotted in black and ISCCP simulated values are multicolored. The color bar indicates the optical thickness data point. Blue (thin), green (moderate), and red (thick) optical depths. The two black horizontal lines indicate where clouds fall in the nine-box plot with respect to cloud top pressure.

cirrus layer detected by the CALIPSO lidar over a mix of clouds ranging from cumulus congestus to fair weather cumulus to an altostratus regime. This situation illustrates a common occurrence in the tropical Pacific, a thin persistent cirrus layer that resides over other types of clouds.

Even though this overpass is from the East Pacific, thin, persistent cirrus is something that seems to be prevalent in both regions. The lower panel displays the CloudSat and ISCCP cloud tops plotted as a function of pressure. The black line indicates the CloudSat detected cloud top heights and the multicolored line is the ISCCP simulated values. Each color indicates the range of optical thicknesses. For example, a value of one (blue) indicates thin optical depth ($0<\tau<3.6$) and two (green) indicates medium optical thickness ($3.6<\tau<23$) and three (red) indicates thick optical depths ($23<\tau<1189$). The thin, medium, and thick nomenclature comes from Jakob and Tselioudis (2005) and is often used to describe the optical depths associated names of the cloud regimes contained (Rossow and Schiffer 1999) within the nine-bin box plot. Also included on the plot are two horizontal lines that indicate the 680hPa and 440hPa pressure heights. These lines demarcate what could be considered low, middle and high clouds to follow the parlance from Jakob and Tselioudis (2003). This is done so as to visually display where in the nine-box histogram these simulated values would fall. It is worthwhile to note that the CloudSat values do not follow the cirrus layer aloft. As mentioned before it was necessary, because of the ubiquitous nature of optically thin cirrus, to exclude tenuous cirrus layers with bases above 15km and/or layers that have an integrated optical thickness of less than one.

Figures 3.3 and 3.4 depict the case study in 42-bin joint P_{top}-τ histograms

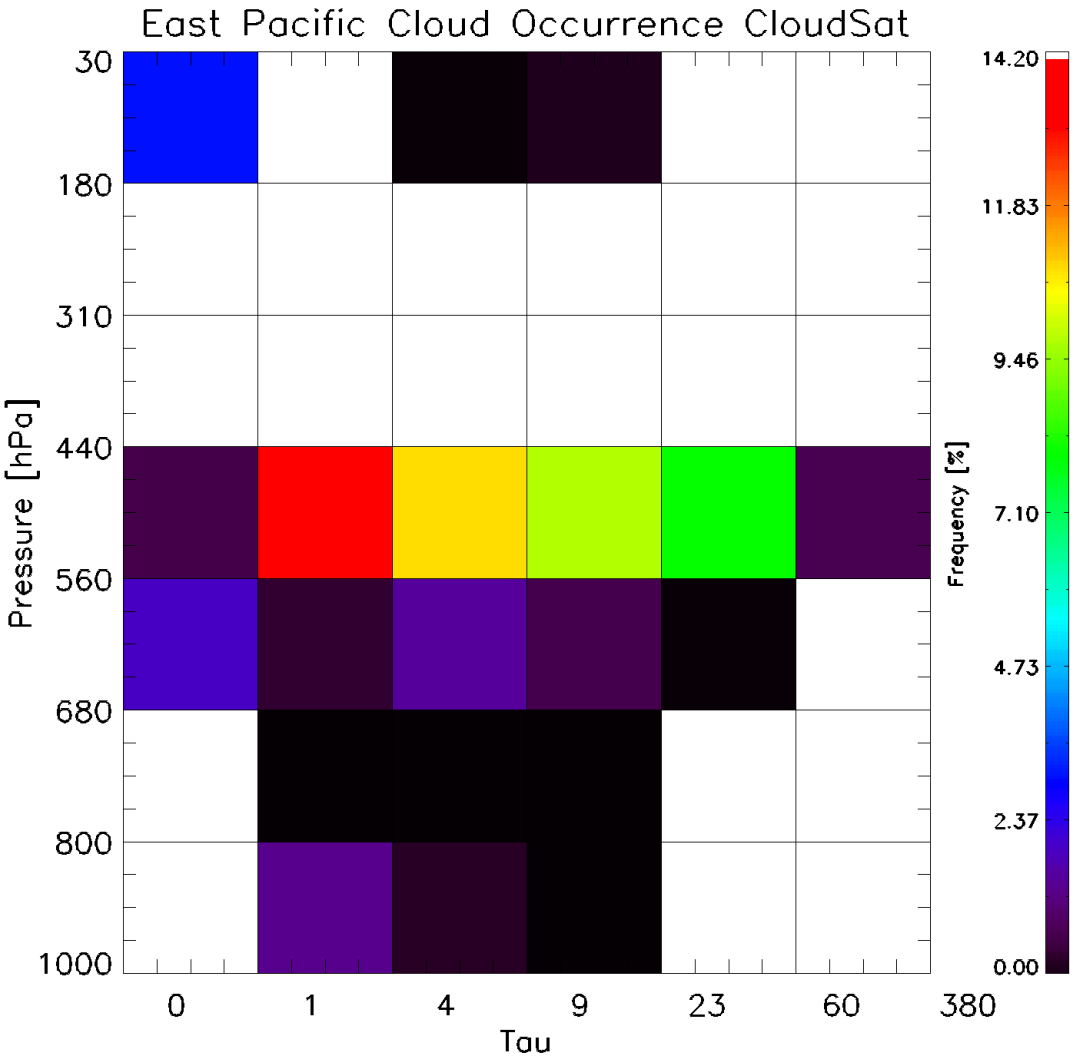

Figure 3.3 The 42-bin histogram plotting frequency as a function of cloud top pressure and optical depth using CloudSat/CALIPSO. Redder colors indicate higher frequency.

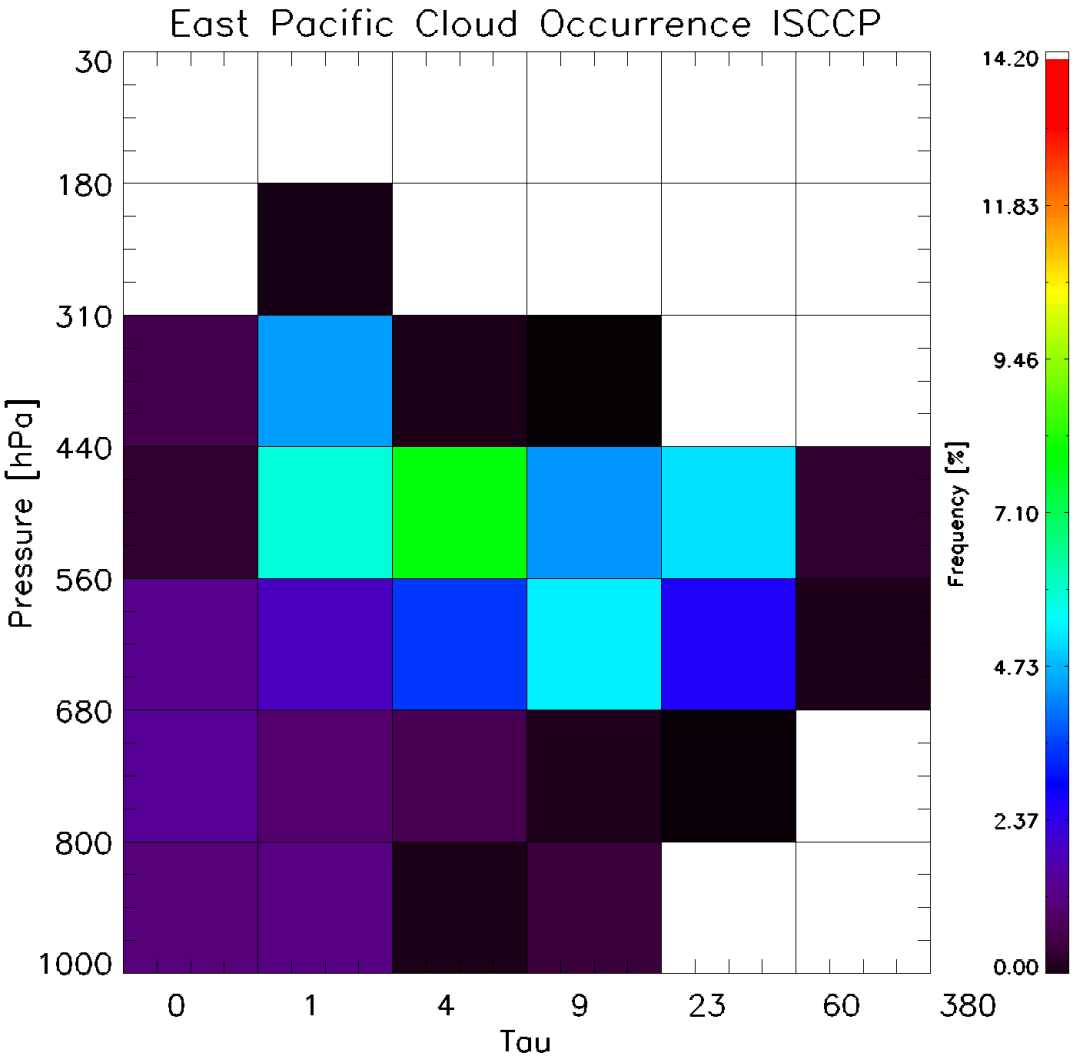

Figure 3.4 The 42-bin histogram plotting frequency as a function of cloud top pressure and optical depth using ISCCP data. Redder colors indicate higher frequency.

compiled using the CloudSat and ISCCP simulated quantities, respectively. As described earlier, we can also take these bins and combine them into coarser nine-bin histograms with each bin assigned a name based on the cloud type it is thought to describe. ISCCP only produces one cloud top pressure per CloudSat profile, but as we can show in the case study, multiple cloud tops can occur and be identified by CloudSat and CALIPSO. Since the ISCCP simulator, like to ISCCP observations, can only detect the upper most cloud top pressure based on the effective radiative temperature, it was necessary for comparison purpose of a first order to only plot the uppermost cloud top pressure detected by CloudSat/CALIPSO. Figures 3.3 and 3.4 depict the CloudSat/CALIPSO and ISCCP cloud top pressure arranged in the 42-bin joint histogram. For example, a CloudSat profile has one cloud top simulated value from ISCCP as well as cloud top and bases identified by hydrometeor occurrence. All tops and bases are plotted (in Figure 3.5) in accordance with the ISCCP cloud type that was identified by the ISCCP simulator for the profile. Therefore, each bin of the nine-bin histogram (Figure 3.5) shows the CloudSat/CALIPSO hydrometeor detected values plotted within the ISCCP defined regimes. The bin that these layers are added to is determined by the ISCCP-simulated value calculated for that particular footprint.

The two histograms quantify the occurrences that are illustrated by the CloudSat pass depicted in Figure 3.2. The majority of occurrences for both figures occur in the middle of the P_{top}-τ diagram. This bin, according to the nine-box histogram would be labeled altostratus. Two major differences are evident from the Figures 3.3 and 3.4. Firstly, CloudSat populates the upper-most cloud top bins while ISCCP does not register occurrences there. This is most likely attributed to the cirrus in the beginning of the

profile that are thick enough to pass the test in the CloudSat algorithm to be identified, but are not detected by the ISCCP simulator. Recall cirrus clouds with bases above 15km and layer optical depth of less than one are omitted in the CloudSat/CALIPSO analysis. Secondly, the ISCCP simulator has populated the lowest optical depth and cloud top pressure bins. This would be referred to as the cumulus bin to follow the nomenclature of the nine-box histogram model in Figure 2.4. This is most likely due to the tenuous cloud layers visible in the CloudSat pass between approximately 7.0˚ and 7.5˚ latitude.

As discussed in the methodology section, these bins can be further combined into a coarser nine-bin histogram. From that we then take each of these bins and plot, as a function of height, the cloud tops and bases as detected by CloudSat/CALIPSO merged product (RL-GEOPROF). Figure 3.5 shows the case study depicted in the nine-box histogram. Within each box the frequency of occurrence of each cloud type defined by ISCCP simulated values is listed. Also listed is the percent of bases and tops that reside above 440hPa. The highest frequency of occurrence lies with the altostratus regime occurring approximately 47 percent of the time (cloud top pressure 680-440 and optical depth 3.6-23.0). For this particular case study, there were no footprints that were classified as deep convection. The altostratus regime appears to be well represented when the tops and bases are plotted within it with only a small amount of what appear to be cirrus over top. The cirrus regime and cumulus regime, on the other hand, are not representative of the actual distribution of hydrometeor layers. In the cirrus regime, there are two modes with the larger one appearing to be low or middle clouds. The cumulus bin is dominated by what would appear to be cirrus over low-level clouds. It is interesting to note that for this particular pass, the cirrus and cumulus bins appear to be inverted.

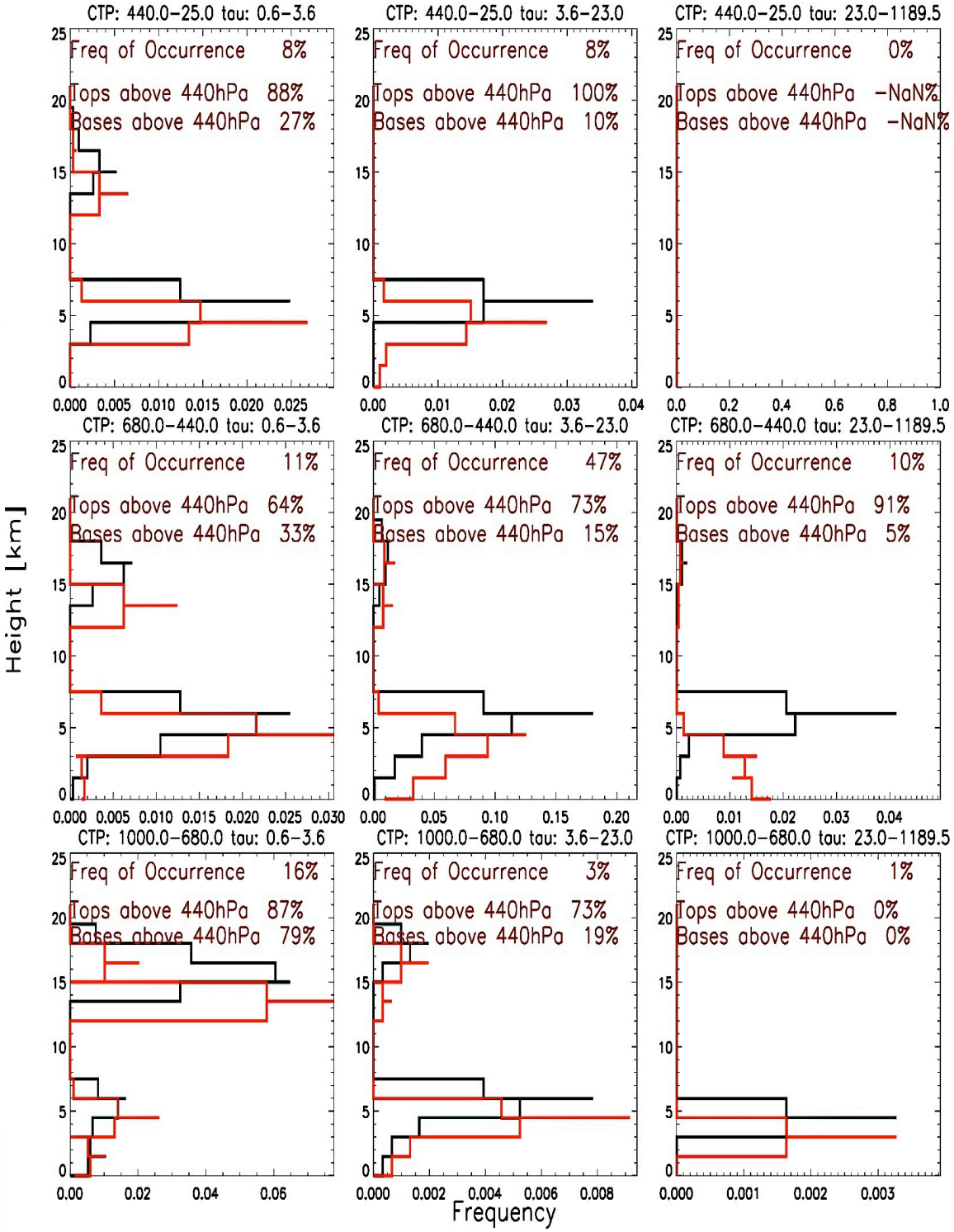

Figure 3.5 Nine-box histogram for 4 February 2007. Within each box the CloudSat tops are plotted in black and the bases are plotted in red. Each box contains the frequency of occurrence of the ISCCP simulated cloud type as well as the percent of tops and bases that are above 440hPa.

Despite the discrepancy in some of the bins, the stratus, stratocumulus, altostratus, and nimbostratus bins seem to accurately represent the regime classification associated with those particular bins.

Figure 3.6 depicts the second case study analyzed. This is an A-Train pass taken from March 3 2007 in the East Pacific. This pass was substantially shorter than the other but displays a good range of different cloud types and also some multiple layers. Figure 3.7 displays the CloudSat reflectivity in the top panel and the ISCCP simulated values and CloudSat tops plotted as a function of pressure. Similarly as before, the cirrus clouds that are visible in the radar reflectivity are not accounted for in the cloud tops plotted by CloudSat/CALIPSO. This is for the same reason as well; the thin cirrus clouds are presumed to be too far beyond the sensitivity of ISCCP and due to their copious nature, must be excluded for comparison. This particular pass illustrates some of the nuances that were implemented for the CloudSat detection algorithm. At the beginning of the pass we can see some cloud structures that are omitted by the CloudSat/CALIPSO product. This is due to a detection bug in CALIPSO for clouds that occur in the boundary layer. Although these structures appear to be a combination of CloudSat and CALIPSO returns, the false detection of CALIPSO for these low-lying thin clouds precluded their use in analysis. The cutoff for these clouds was cloud tops below 3km and a layer optical depth less than one.

Similar to the first case study, the cloud tops and bases can be collected and arranged into 42-bin histograms. Figures 3.8 and 3.9 display the histograms for CloudSat and ISCCP simulated frequencies, respectively. An interesting point for the overall shape of the histogram is that cloud top frequencies have not only moved downward to higher

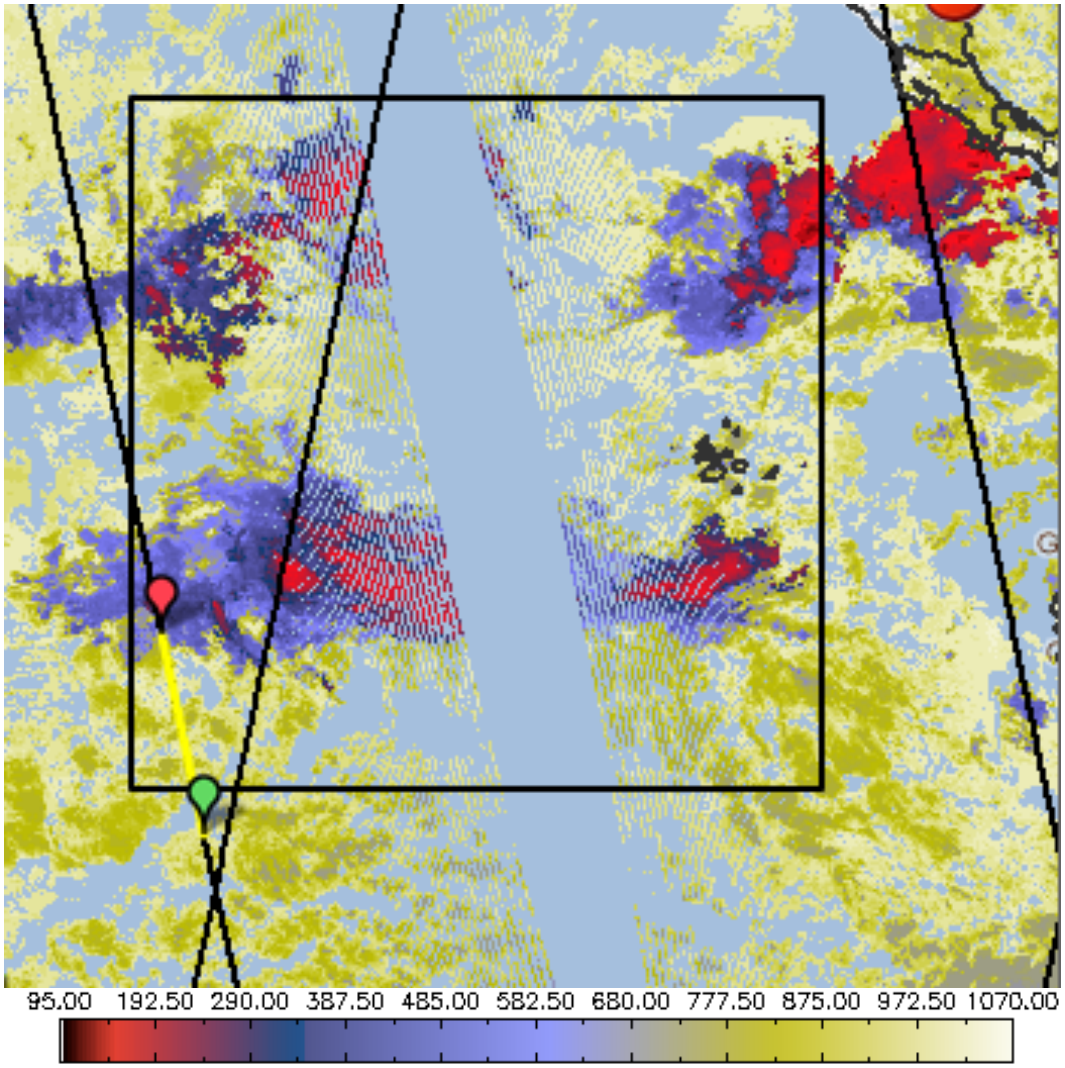

Figure 3.6 Map showing the area in the East Pacific within the black outline of the box. The diagonal lines running through the map are CloudSat passes. Lines that are skewed left with respect to the bottom of the map are ascending passes. Conversely, the other lines represent descending passes. The two pins, green and red, represent a portion of the of the CloudSat pass through the region. Superimposed are cloud top temperatures provided by MODIS aboard Aqua. The pass is from March 3 2007 (day of year 62)

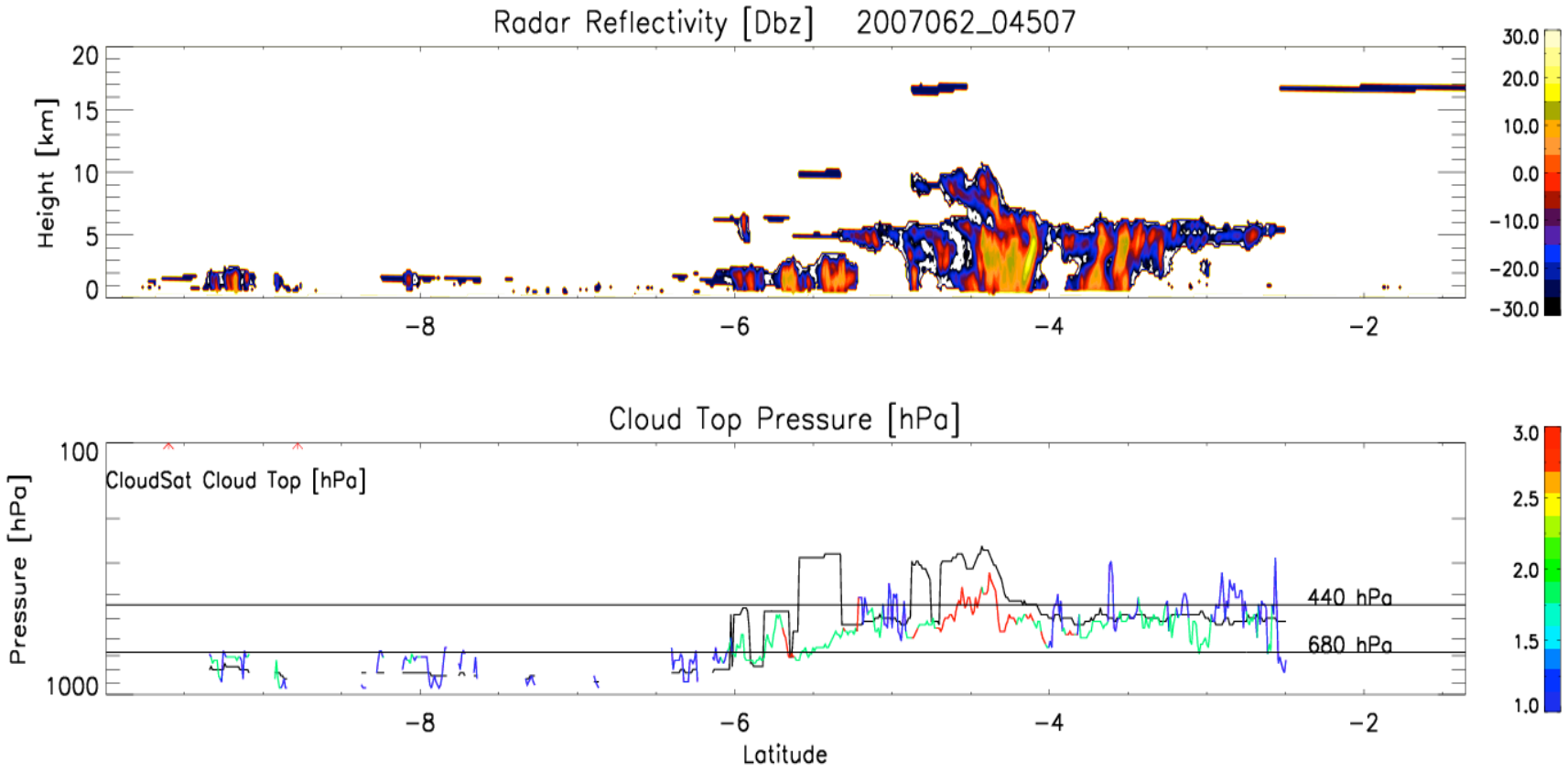

Figure 3.7 R-L GEOPROF profile from 3 March 2007. Top panel displays CloudSat dBZ and CALIPSO plotted as a function of height and latitude (time). Bottom panel displays CloudSat and ISCCP cloud tops plotted as a function of pressure and latitude (time). CloudSat cloud tops are plotted in black and ISCCP simulated values are multicolored. The color bar indicates the optical thickness data point. Blue (thin), green (moderate), and red (thick) optical depths. The two black horizontal lines indicate where clouds fall in the nine-box plot with respect to cloud top pressure.

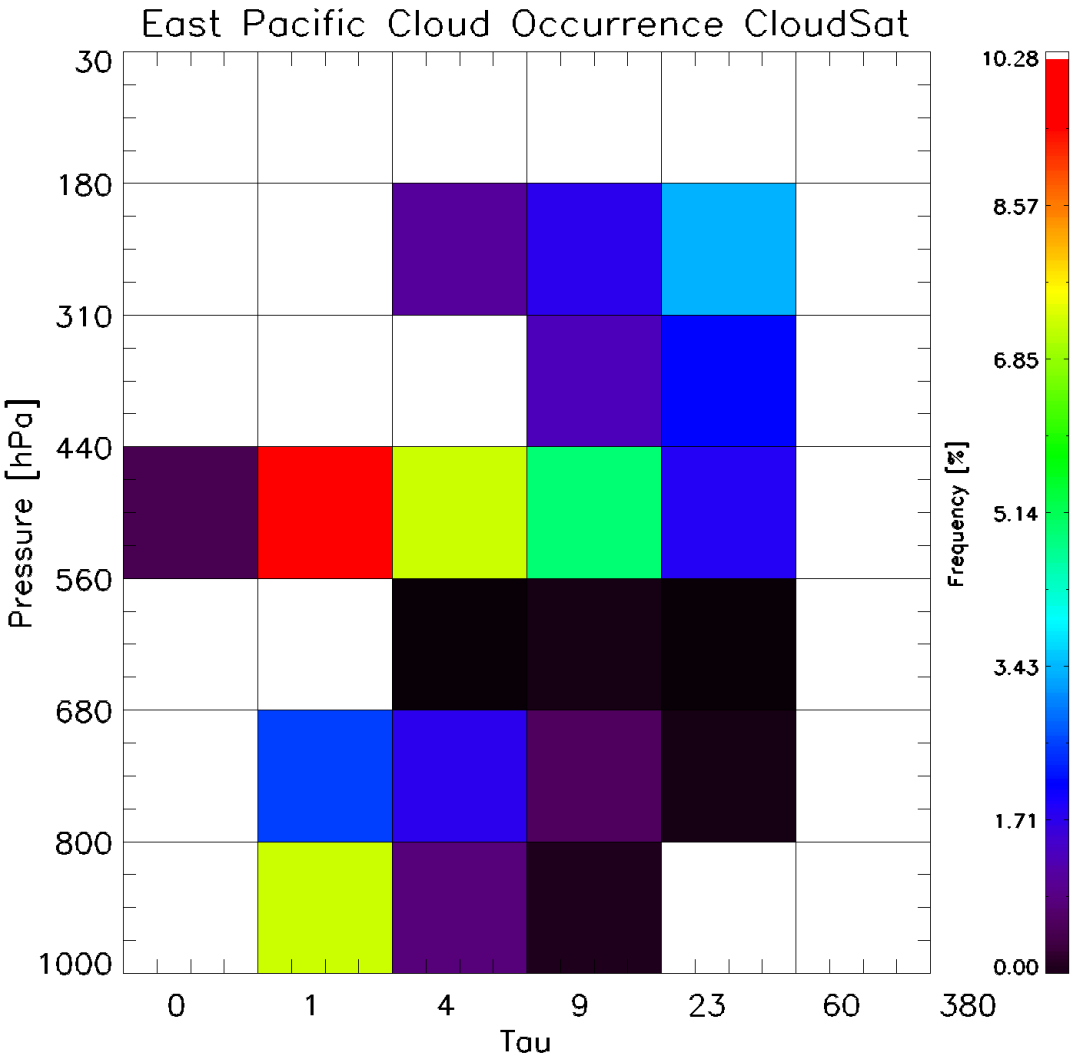

Figure 3.8 The 42-bin histogram plotting frequency as a function of cloud top pressure and optical depth using CloudSat/CALIPSO data. Redder colors indicate higher frequency.

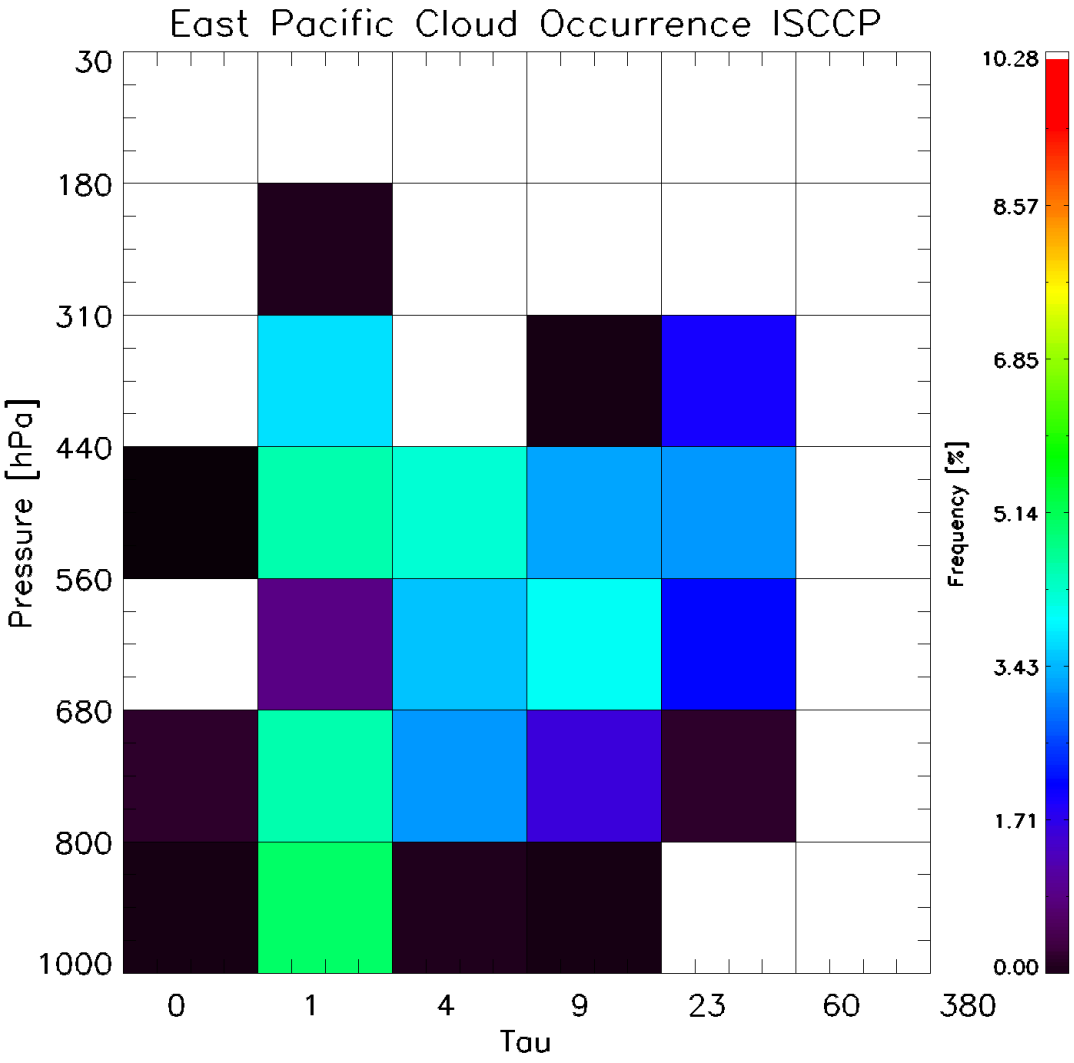

Figure 3.9 The 42-bin histogram plotting frequency as a function of cloud top pressure and optical depth using ISCCP data. Redder colors indicate higher frequency.

cloud top pressures (lower altitude) but also toward smaller optical depths. It is worthwhile to take note of what would be called the cumulus bin between the two. The CloudSat bin does not register any occurrence for the thinnest optical depth and highest cloud top pressures. However, the frequency of the cumulus bins between ISCCP simulated data and CloudSat data is approximately the same. This implies that clouds from higher bins (higher in the atmosphere) have been shifted down from the CloudSat detected occurrences when compared to the ISCCP simulated bins.

Just as in the first case study, these histograms can be combined to form the nine-box histograms, as seen in the Figure 3.10. There is good agreement between the coarse nine-box histogram names assigned here and the actual distribution of cloud layers. An interesting point is that the higher cloud bins, cirrus and cirrostratus, contain a single layer although this layer is perhaps not as high in altitude as they are more likely to be. It is worthwhile to note although these distributions may not perfectly describe the bin and naming convention associated with it, that it may take a larger sample to converge on a more concise distribution.

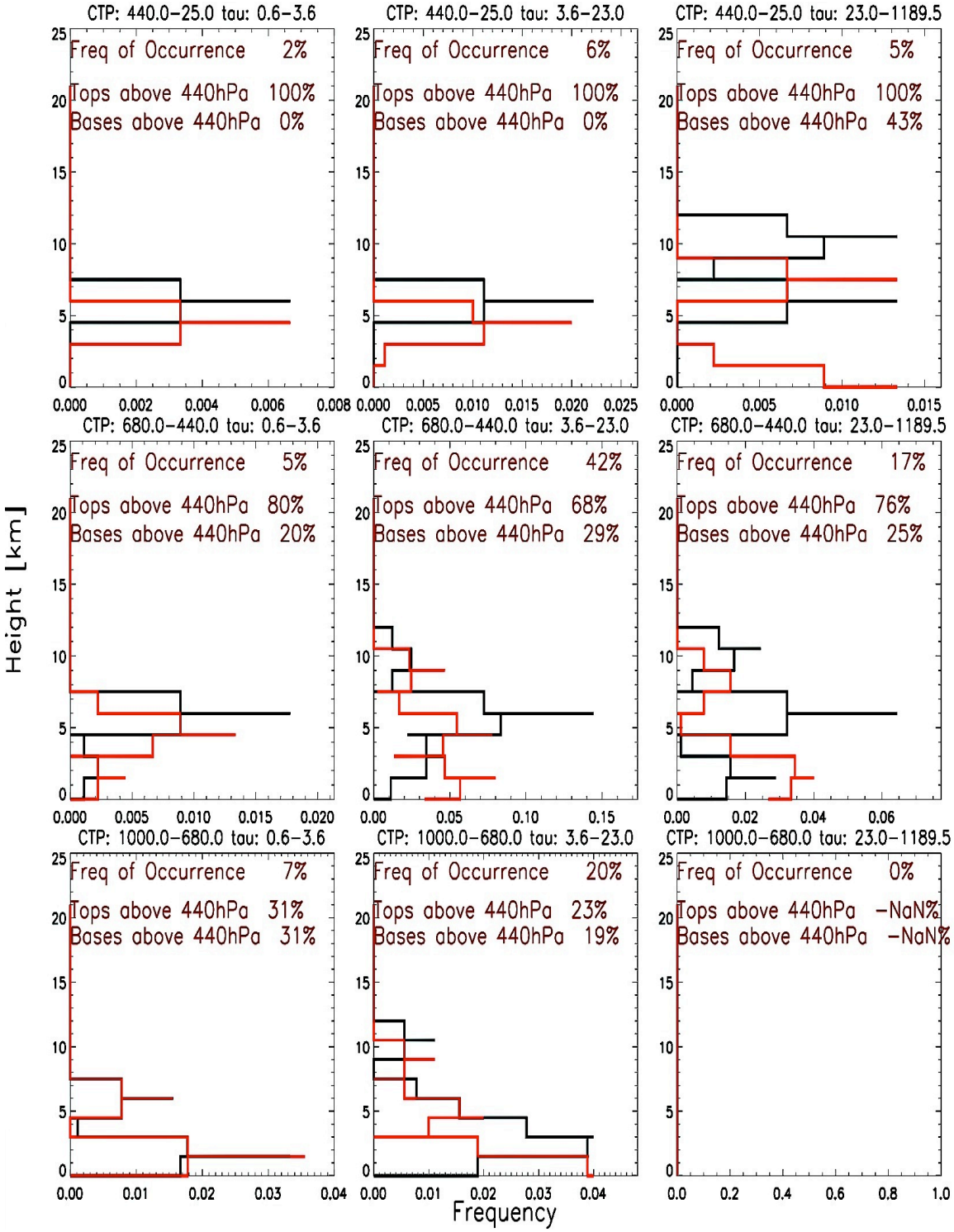

Figure 3.10 Nine-box histogram for 3 March 2007. Within each box the CloudSat tops are plotted in black and the bases are plotted in red. Each box contains the frequency of occurrence of the ISCCP simulated cloud type as well as the percent of tops and bases that are above 440hPa.

CHAPTER IV

RESULTS

The following figures were produced using the same method as described in the case study section. First it was necessary to build the 42 bin plots as before to test the robustness of the simulator and establish a base line with which to compare the actual uppermost cloud top detected by CloudSat to that which the ISCCP simulator produces. The figures were produced using detected and simulated values from 2007 profiles containing cloudy scenes. Figures 4.1 and 4.2 contain the 42-bin box histograms for the West Pacific. The CloudSat figure as well as the ISCCP simulated figure (West Pacific) show a bimodal distribution with one mode at higher cloud top heights and the other at lower cloud top heights. The CloudSat figures shows that the mode at lower cloud top pressures (higher altitudes) is much higher than the secondary maximum among the higher cloud top pressures (lower altitudes). This likely indicates that cirrus clouds dominate the West Pacific. The dominance of cirrus clouds is still apparent in the West Pacific even though TTL cirrus were excluded from this study. This is presumed to be due to the outflow of cirrus from the copious deep convection in the West Pacific. ISCCP simulated values show the maximum in frequency of occurrence of cloud tops in the bins just below the upper most cloud top bins. It is worthwhile to note that, even though the maximum is one bin lower within the ISCCP simulated plot, it still will fall

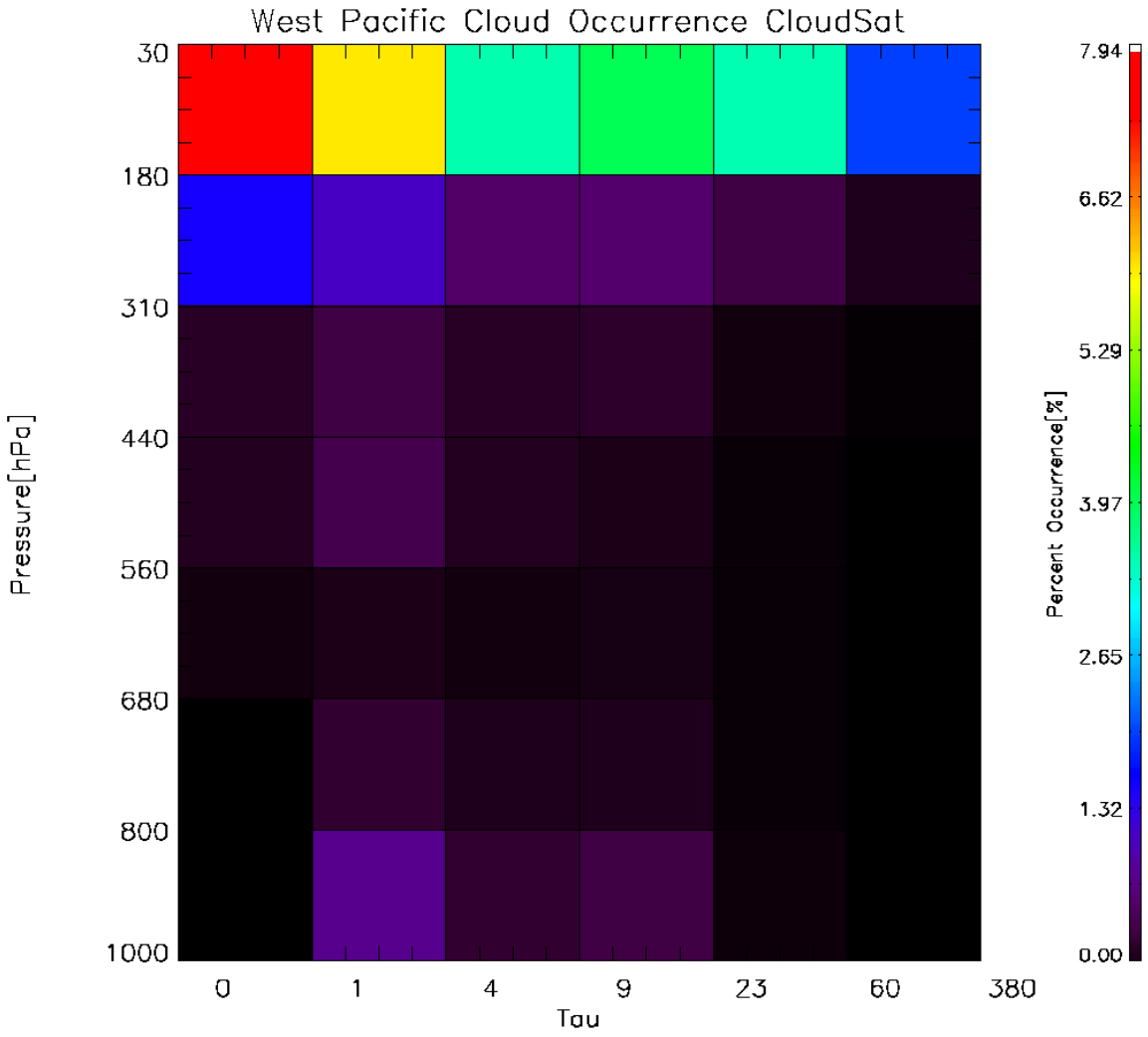

Figure 4.1 The CloudSat detected cloud tops for the West Pacific for the entire year of 2007.

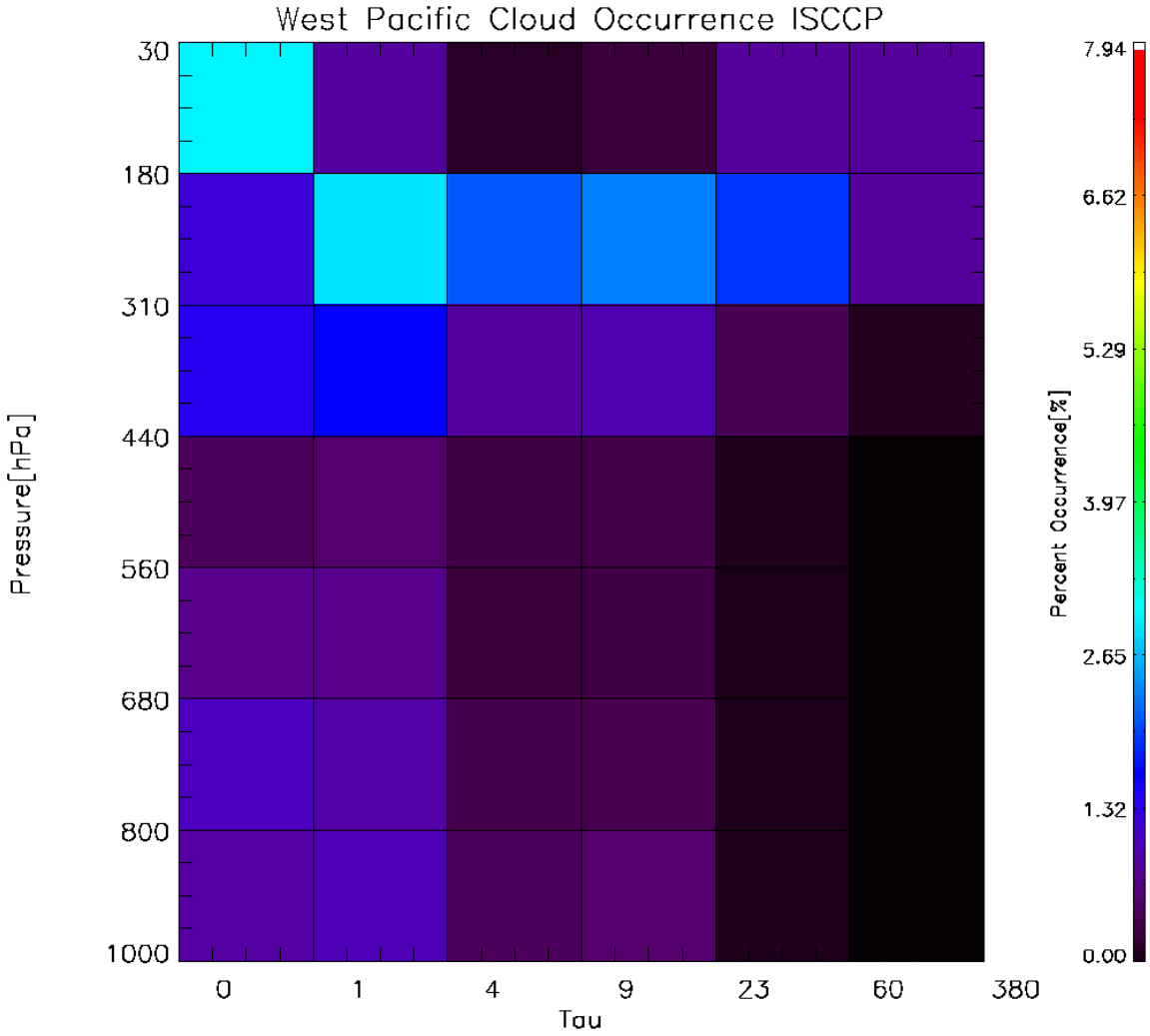

Figure 4.2 ISCCP simulated values for the West Pacific for the entire year of 2007.

within the same bins when they are combined to form the coarser nine-bin histograms. This alludes once again to the impetus of this study; does the naming convention allocated to these coarse bins preclude an actual quantitative understanding of what is actually contained inside these bins? The largest maximum for the ISCCP figure is in the upper left hand of the diagram in the lowest optical depth bin and lowest cloud top pressure (thin and high in the atmosphere). This is assumed to be an artifact of the simulator and in accordance with the ISCCP values. This same maximum can also be seen in Hartmann 2001 (Figure 2.2). Since the data used to detect cloud top pressures via CloudSat also incorporate CALIPSO lidar data, it could be surmised that the higher cloud top pressures from CloudSat are due to the detection of thin cirrus below the threshold of ISCCP. These clouds are most likely not thick enough to approximate an emissivity of one, yet are thick enough to provide a non-zero radiative contribution to the profile. Thus, ISCCP would mark a cloud top somewhere lower in the atmosphere depending on the scene beneath the thin cirrus. As alluded to before, TTL cirrus clouds are ignored for this figure. They are ignored not because they are radiatively insignificant, as there is ongoing debate as to their radiative importance, but because of their relative dominance. Even with this omission, the relative dominance of cirrus clouds of all optical thicknesses is apparent. Just as was seen in the case studies, the cumulus regime is much more populated within the ISCCP simulated figure than for the CloudSat figure. This is surmised to be the movement of cloud occurrence from either the lower bins (lower in the atmosphere or high P_{top} values) into higher bins (higher in the atmosphere or low P_{top} values) from CloudSat, or conversely, from the higher cirrus bins to the lower cumulus bins. This is also apparent by observation of the two modes from the ISCCP simulated

figure. There are two modes like there are in the CloudSat figure, however, with two distinct differences. One is that the frequency of occurrence within the mode in the higher bins is much more concentrated for CloudSat than it is for ISCCP, especially in the upper most cloud top pressure bins. The second is that the mode in the lower bins is smaller in CloudSat than it is in the simulated values. In other words, the simulated values tend to spread out the frequencies of occurrence about the modes that are detected in the CloudSat figures.

Figures 4.3 and 4.4 for the East Pacific show a distribution markedly different from that of the West Pacific. CloudSat shows that there are two maxima, much like in the preceding figures; there is one mode in the uppermost cloud top pressure bins from low to high optical thickness and one in the lowest cloud top pressure bin for thin to moderate optical thickness. It is interesting to note that the East Pacific appears to be the inverse of the West Pacific with its largest mode occurring low in the atmosphere and the lower maximum occurring high in the atmosphere with regard to CloudSat. Higher cloud top pressures in the East Pacific could be attributed to the lower sea surface temperatures that tend suppress convection, especially in comparison to the West Pacific.

The simulated values show the largest maximum along optical thicknesses from thin to thick is one bin higher than that of CloudSat. This effect is thought to be caused by the temperature inversion that commonly occurs in the East Pacific. There is also a maximum for the upper most cloud top pressure bins for thin cirrus clouds. As mentioned before, boundary layer clouds of optical thickness less than one-half and residing lower than three kilometers in the atmosphere were eliminated due to false positive cloud detection by CALIPSO. Although this issue has been resolved as of late, it is still seen in

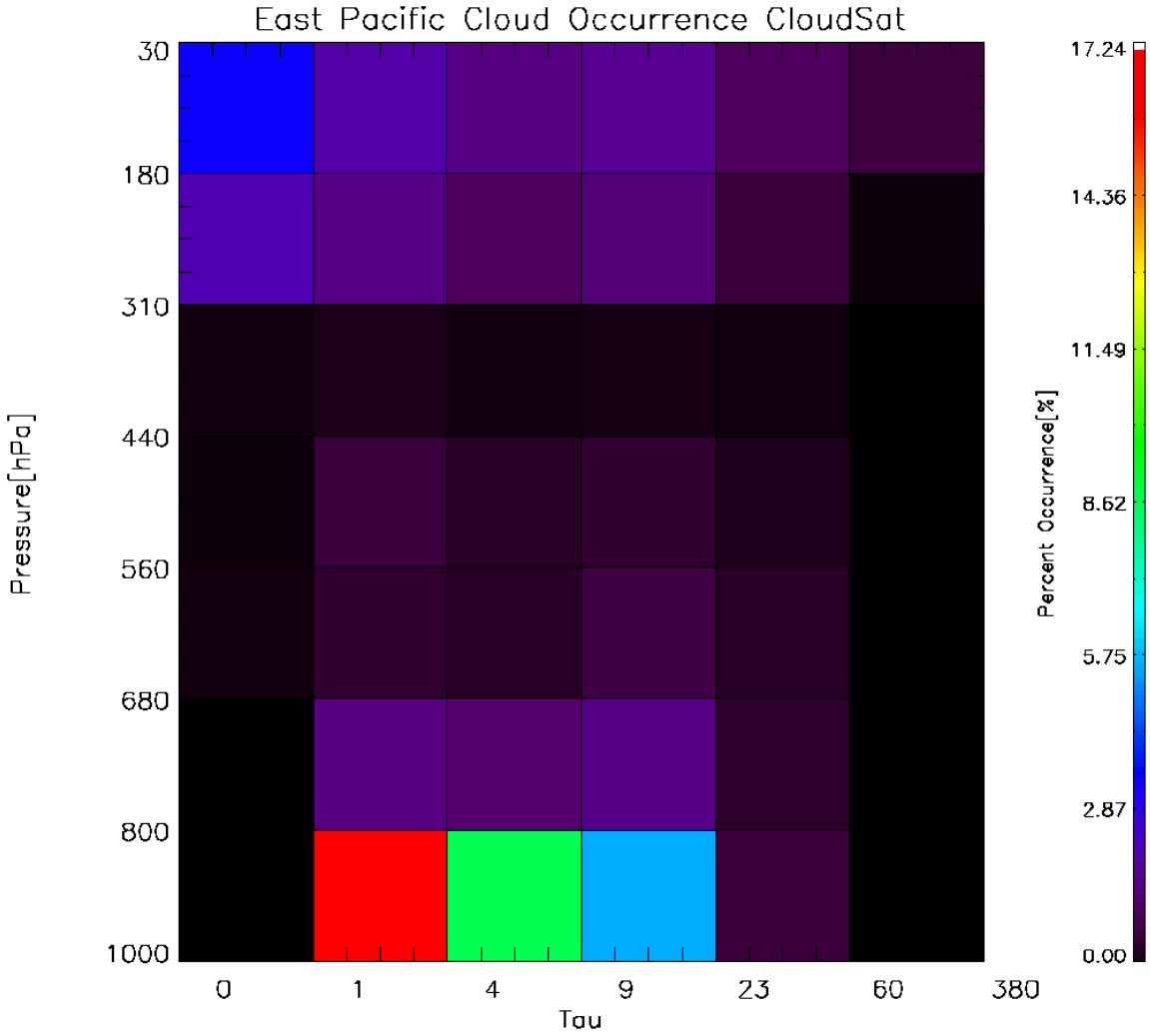

Figure 4.3 The CloudSat detected cloud tops for the East Pacific for the entire year of 2007.

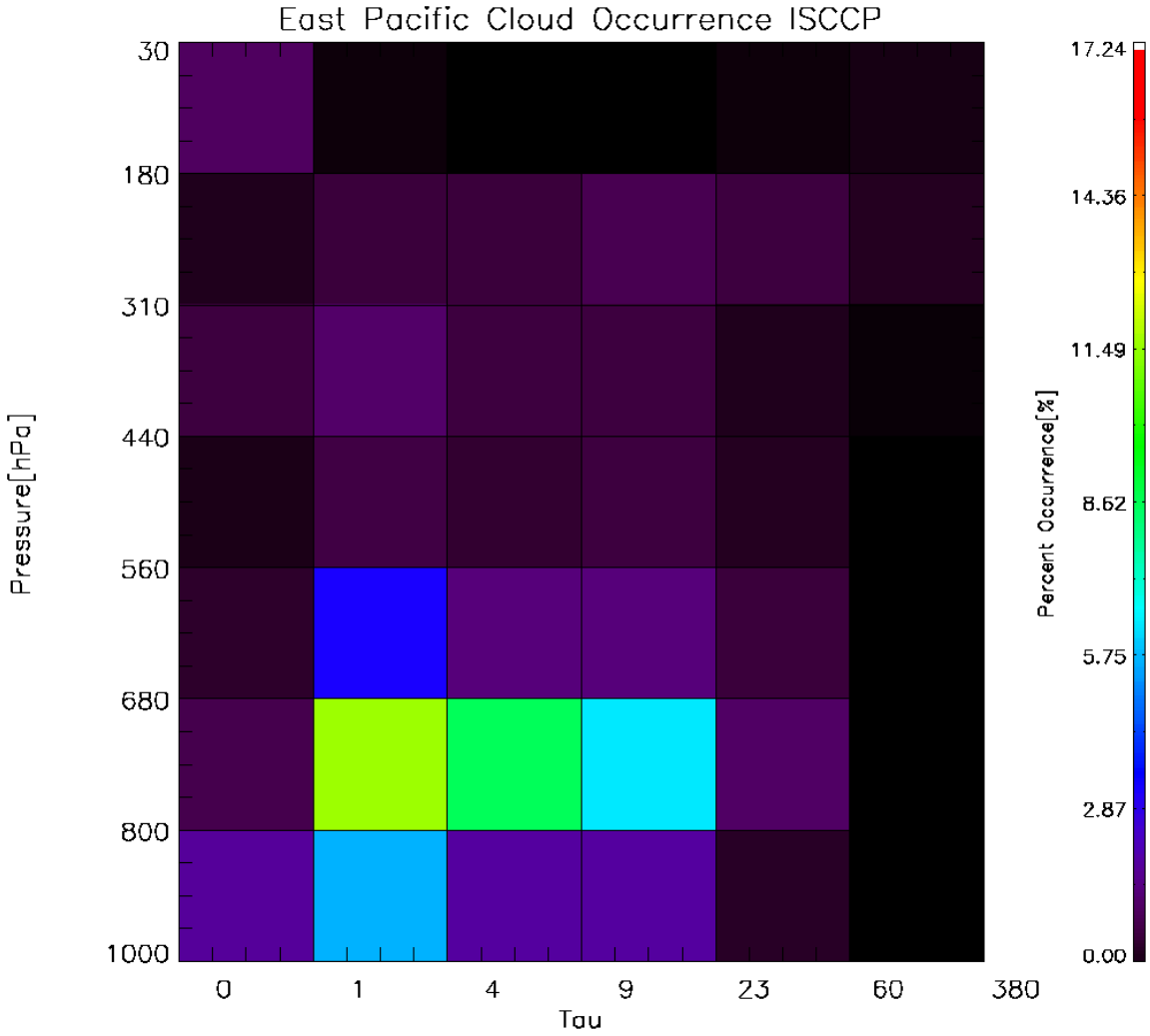

Figure 4.4 ISCCP simulated values for the West Pacific for the entire year of 2007.

the years covered by this study. It is also interesting to note that the East Pacific ISCCP simulated values also appear to be an inverse of the West Pacific ISCCP simulated values.The findings from this initial analysis are similar to that of Jakob and Tselioudis (2003), which compared active remote sensing observations to ISCCP observations. Our analysis shows that some of the cloud regimes as described by ISCCP may be single-layer description of multilayered cloud scenes, i.e., ISCCP is only able to sense the upper-most cloud top. The data that are shown in Jakob and Tselioudis (2003) may reinforce our finding, but could also be attributed to other differences. One difference is the RFO from Jakob and Tseliousdis (2003) could be due to the use of radar and lidar at the ARM site, especially if the ability of the radar and lidar to penetrate into convective regimes is utilized.

The next step to take in our analysis was to plot the occurrences of hydrometeor layers detected. Figures 4.5 and 4.6 display the vertical distributions of hydrometeor occurrence for various maximum values of radar reflectivity from the RL-GEOPROF data for the East and West Pacific, respectively. The West Pacific study region exists in the upwelling portion of this circulation where warm sea surface temperatures contribute to the production of deep precipitating clouds and a high coverage of thick cirrus. In the East Pacific, a cooler sea surface and large-scale subsidence result in shallow convective clouds, less precipitation, and less cirrus although the East Pacific ITCZ does migrate through this domain. These figures confirm the findings from the previous joint histograms in their overall shape. The West Pacific has the largest occurrence of hydrometeor layers in the upper atmosphere at all detected dBZ thresholds while the East Pacific appears to be the inverse with the largest hydrometeor occurrences in the lower

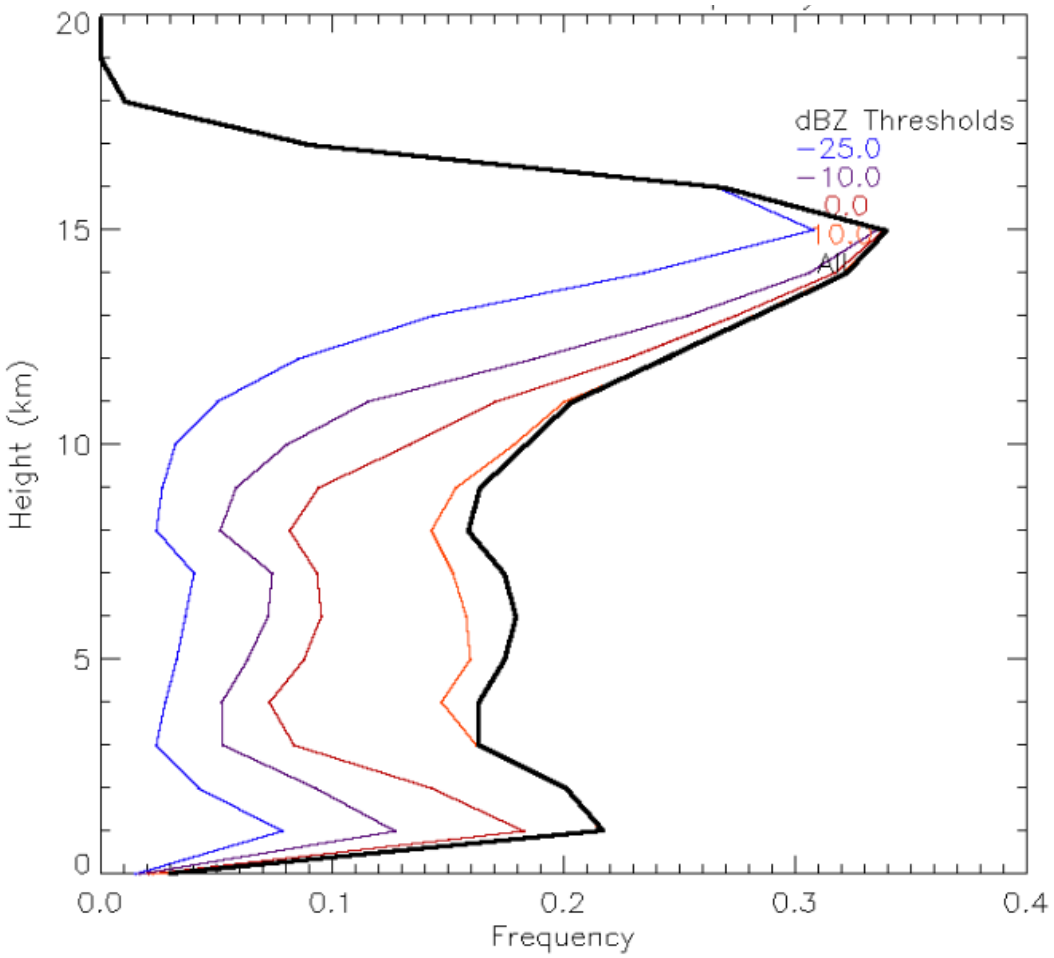

Figure 4.5 Hydrometeor occurrence as a function of height in the West Pacific for 2007 from the CloudSat RL-GEOPROF product. The different lines indicate different dBZ maximum thresholds while the dark black line indicates all occurrences.

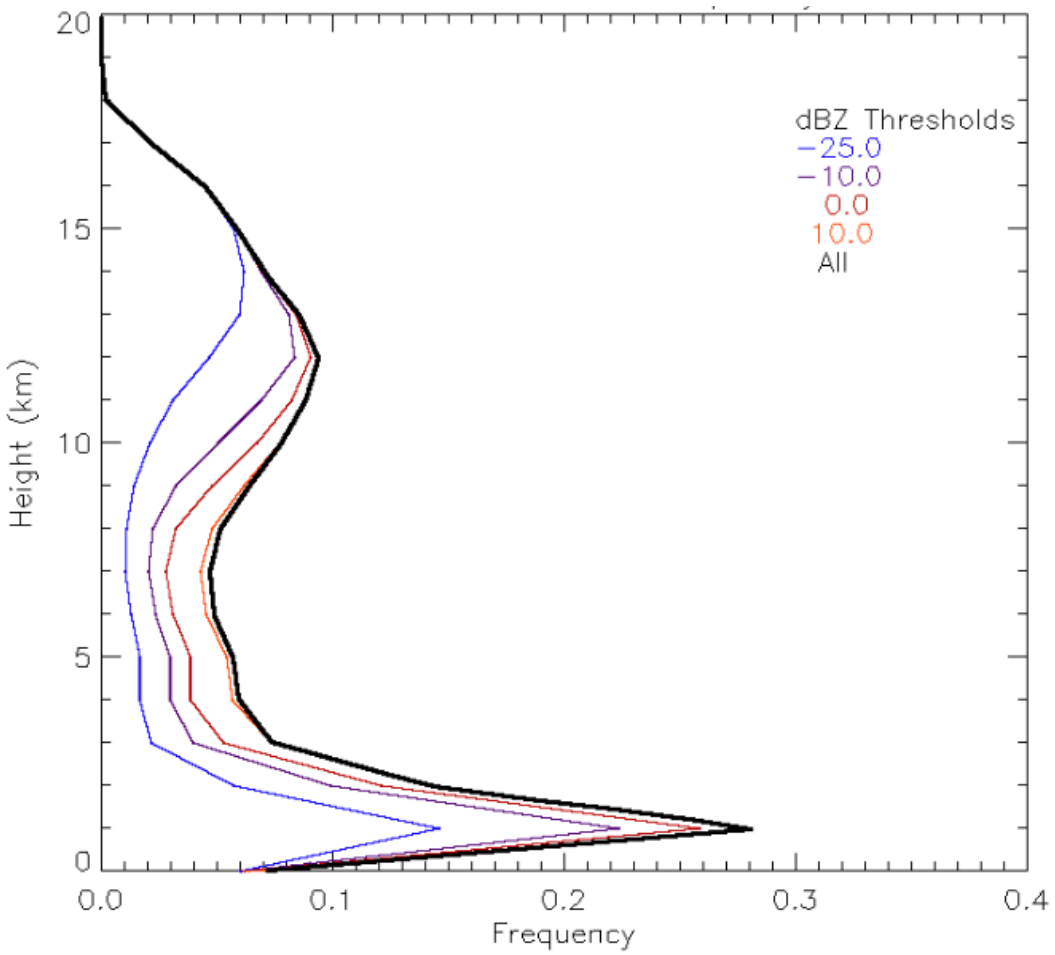

Figure 4.6 Hydrometeor occurrence as a function of height in the East Pacific for 2007 from the CloudSat RL-GEOPROF product. The different lines indicate different dBZ maximum thresholds while the dark black line indicates all occurrences.

part of the atmosphere. Additionally, the figure from the West Pacific the total cloud cover is found to be 75% (47% of the columns are multilayer). Not only do we find a larger occurrence of hydrometeors in the middle troposphere but also a greater fraction of these clouds occur at larger values of radar reflectivity indicative of more extensive precipitation. The West Pacific displays two distinct modes with a lesser mode in the middle troposphere. Note that as much as half of the hydrometeor occurrences in the middle troposphere are found to have radar reflectivity factors in excess of -10 dBZe. In the East Pacific where the total cloud cover is 74% (32% of the columns are multi-layer) the vertical distribution of hydrometeor occurrence is distinctly bimodal and there is much less indication of precipitation.

The next group of figures (4.7 and 4.8) shows a coarser representation of the 42-bin classification. It follows the work of Rossow and Schiffer (1999) that uses nine bins labeled as to what cloud type they most likely represent. The cloud tops and bases are recorded and binned according to the ISCCP simulated value for a given profile. In other words, all CloudSat layers as detected by hydrometeor occurrence are cast into the framework of the nine-box histogram. The location of the data point in the nine-box histogram is based on the ISCCP simulated values for each footprint. Each figure shows cloud tops in black and cloud bases in red. The layers are plotted within these bins as a function of physical height, or height from the surface in kilometers. This allows for a more meaningful interpretation of what lies within these bins as a function of height. As in the case study section, the frequency of occurrence is based on how frequently the ISCCP simulator detects that particular bin versus the other nine bins. Also included is the percent of tops and bases that reside above 440hPa relative to the cloud occurrences

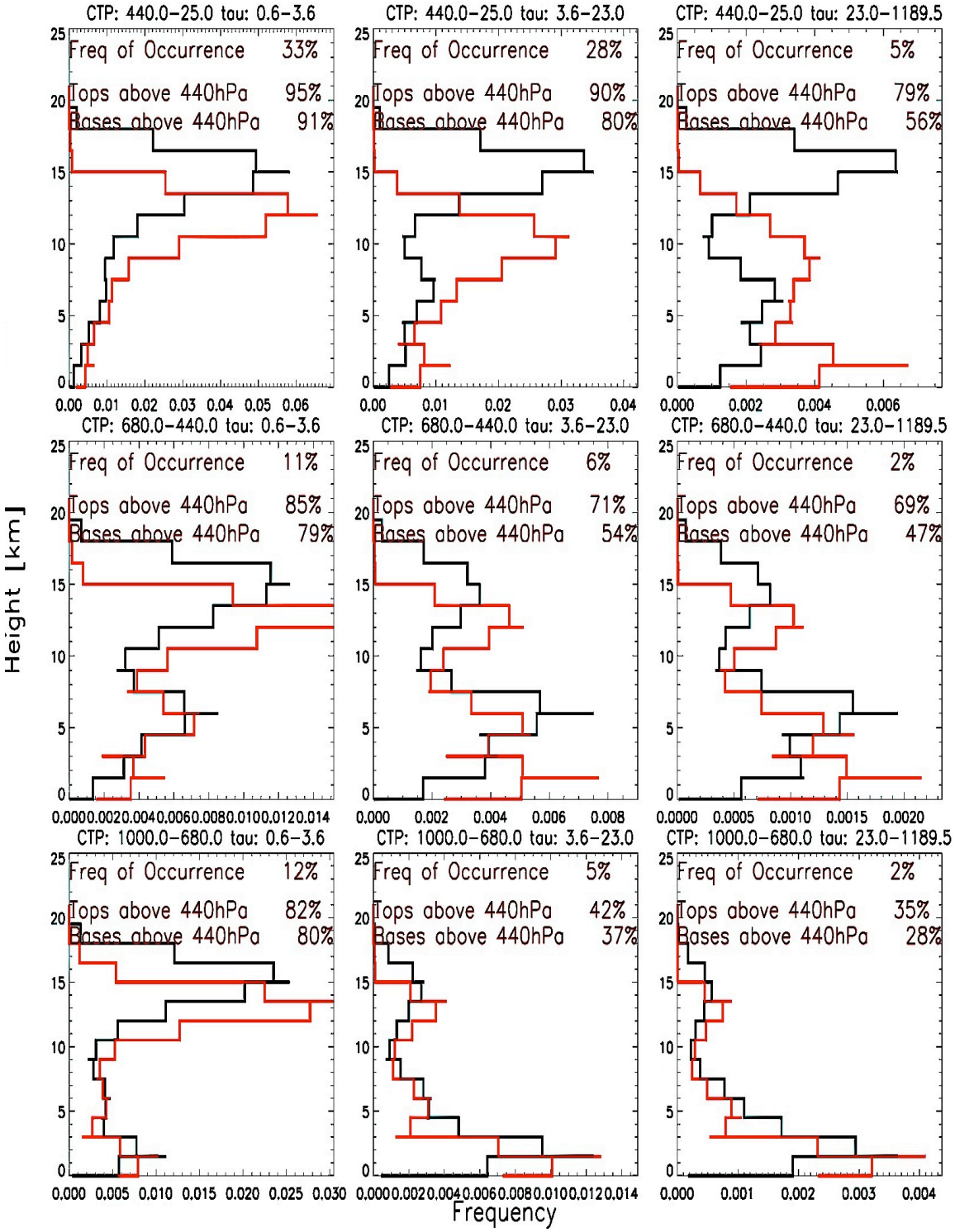

Figure 4.7 Hydrometeor layer occurrence detected by CloudSat for the West Pacific. Cloud tops are in black and cloud bases are in red. Cloud layers are placed into bins based on the ISCCP simulated value for a given CloudSat footprint. In other words, if the ISCCP simulator identifies a cloud top pressure higher than 680hPa and an optical depth less than 3.6, then those CloudSat layer(s) are plotted in the bottom left-hand bin, referred to as cumulus by Rossow and Schiffer 1999.

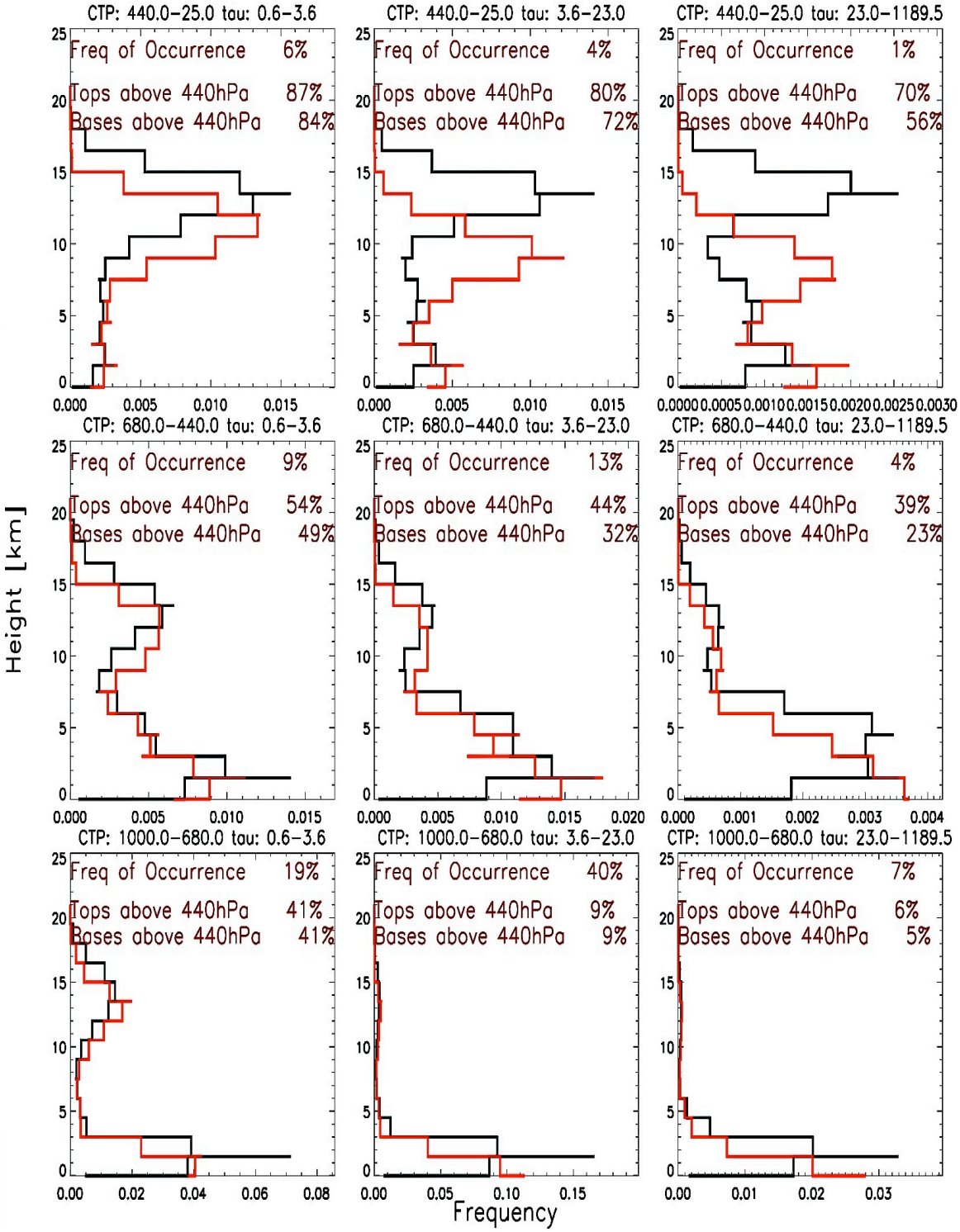

Figure 4.8 Hydrometeor layer occurrence detected by CloudSat for the East Pacific. Cloud tops are in black and cloud bases are in red. Cloud layers are placed into bins based on the ISCCP simulated value for a given CloudSat footprint. In other words, if the ISCCP simulator identifies a cloud top pressure higher than 680hPa and an optical depth less than 3.6, then those CloudSat layer(s) are plotted in the bottom left-hand bin, referred to as cumulus by Rossow and Schiffer 1999.

that occur for that particular bin.

Analysis of these plots reveals some interesting features. There are some bins that are in good agreement with the naming convention that has been assigned to them, e.g., cirrus and stratus. In the West Pacific, cirrus occurs most commonly at approximately 32% of the time, of which about 90% of the cloud layers reside above 440hPa (higher in the atmosphere). In the East Pacific exhibits good agreement within the cirrus bin with about 80% of the cloud layers detected in the cirrus bin residing above 440hPa. However in the East Pacific, the cirrus is not the most commonly simulated cloud type as in the West Pacific with only approximately 5% of the total simulated footprints within the cirrus bin. This similarity is also seen in the stratus bin within the West and East Pacific. Both regions do not record many instances (1.25% and 7%, respectively) however both have a majority (66% and 95% respectively) of cloud layers that occur below 440hPa.

Despite the good agreement between these particular bins and their associated nomenclature, there are other bins that appear more dubious. The altostratus bin for example (center bin), in the West Pacific shows a definite bimodal distribution with about one-third of the time layers occur completely above 440hPa. This indicates that 33% of the time there is cirrus over some lower layer in the West Pacific. Perhaps of a greater concern is the good agreement in the East Pacific within the altostratus bin. The presumed cirrus layer over low-level clouds is much smaller in the East Pacific altostratus bin. There is a distinct difference with the altostratus bin between the two regions. One interesting point to note is the deep convection bin (top right) in both the West and the East Pacific. It displays several different cloud types mixed together. The distribution is certainly bimodal in nature, although the bases and tops do not move in

lockstep with one another. The maximum occurs in the cloud top above 13km, but the maximum for the bases occurs below 4km. There are secondary maxima for the tops and bases inside the other two, larger maxima. This would indicate that the bin is populated by a wide range of cloud types, e.g., deep convection, in which the maximum for the tops matches that of the maximum of the bases, as well as outflow cirrus from aging convective systems and even some combination of cirrus over low-level clouds.

As mentioned before in the introduction, several studies have been conducted to evaluate model deficiencies. Soden and Vecchi (2011), for instance, find that a great deal of the intermodel uncertainty in GCMs can be attributed to low level clouds. It is then interesting to note the stratocumulus regime in the East Pacific (Figure 4.7). This particular bin appears to be an accurate representation of what one would expect this regime to represent. Less than 10% of the hydrometeor occurrences are in the upper atmosphere. When compared to the West Pacific, it is clear that a slightly different situation exists. Approximately 35% of the hydrometeor occurrences occur in the upper atmosphere in this bin. Although this is not as accurate a representation of the bin as the East Pacific represents, what is of more import is the difference between the two. The differences here reveal, in part, a possible source of uncertainty associated with low-level clouds. The cloud bin, at least in terms of application in GCMs, is treated as a unique description the stratocumulus cloud bin. However, when we observe this situation in the East versus the West Pacific, we see that the hydrometeor occurrences are non-unique. In other words, the application of this cloud bin in the context of model parameterizations treats this particular bin as though it were unique, distinct, and consistent regardless of the region with which it may be associated. Granted this particular study only considers

these two regions and a more rigorous survey must be undertaken, but this problem raises interesting questions about the fidelity of the regime classifications within models. Another bin that shows a great deal of interregional discrepancy is the cumulus bin, lending further credibility to this question of low level cloud representation in models.

CHAPTER V

CONCLUSION

It is almost a certainty that the active remote sensors in the A-Train are ideal for mapping the vertical distributions of hydrometeors as well as their microphysical and radiative properties. However, passive remote sensing data sets like ISCCP and MODIS will remain central to our understanding of the statistics of clouds on Earth and remain a critical component of understanding our skill at simulating clouds in global models. Not only will the global ISCCP record continue to grow beyond its current 3 decades and be augmented by other similar data sets, there are currently no plans by NASA to replace the aging active remote sensors of the A-Train before the mid 2020's.

As a radiative quantity, P_{top} is a function of the distribution of condensate throughout the atmospheric column. It has been understood that the vertical distributions of clouds within the ISCCP P_{top} -τ bins would not correspond identically to the cloud types that these bins are often taken to represent (Rossow and Schiffer, 1999). The actual vertical distributions of clouds are within the ISCCP P_{top} -τ bins are not well documented. We have attempted such an exercise here by simulating ISCCP P_{top} using a component of the ISCCP simulator known as ICARUS and using retrieved τ along the track of CloudSat and CALIPSO.

The ISCCP simulator was run in conjunction with A-Train profiles with good agreement to previous work that provided measurements from ISCCP by Hartmann et al (2001) and Jakob and Tselioudis (2003), as evidenced by comparison of joint histograms. These joint histograms are arranged in the classic 42-bin diagrams arranged by cloud top pressure (P_{top}) and optical depth (τ). These bins according to ISCCP are then condensed into a coarser nine-bin arrangement and plotted according to height using cloud layers and optical depths detected by CloudSat, an active remote sensor. They show that the actual distribution of cloud tops and optical depths is more complex than what was originally thought. Cloud type classification defies a simple interpretation that was yielded from previous studies.

Chen and Del Genio (2009) note: "ISCCP CTP-TAU (P_{top}-τ in this study) histograms are neither what they were intended to be (a distribution of highest cloud top heights) nor what they are sometimes mistaken to be (an actual vertical distribution of clouds), but are instead a hybrid of both". We have found that to be true to varying degrees in the Eastern and Western Pacific Study regions. Based on the observed vertical distributions of hydrometeor layers within the P_{top} -τ bins, we have found that the upper troposphere bins do indeed contain primarily cirrus of increasing geometric thickness as τ increases. However, caution should be exercised in interpretation of these statistics. For example, the cirrostratus and deep convection P_{top} -τ bins in regions where low level clouds are known to occur in conjunction with cirrus (i.e. the regions studied here and the maritime storm tracks of both hemispheres; see Mace, 2010) should be used with caution because semi-transmissive cirrus overlying reflective low level clouds could easily be diagnosed as optically thicker cirrus. It also seems clear that while the ISCCP upper

tropospheric P_{top} -τ bins contain mostly cirrus, not all cirrus are contained in the P_{top} -τ bins by any means. Cirrus layers remain a significant component of the vertical distribution of clouds in every P_{top} -τ bin in the West Pacific Study region. With the exception of the stratocumulus and stratus P_{top} -τ bins in the East, P_{top} -τ bins at pressures larger than 440 hPa do not identically describe any particular cloud type in either of the regions but are mixtures of various cloud types whose properties conspire to produce similar radiative properties.

Cloud parameterizations used in climate models have been based on what could be considered a dubious naming convention. The results in this study have shown that within a given cloud type, there lies the possibility of an entire distribution of cloud layers. Before these cloud types are used in model parameterizations a true quantitative understanding of what actually exists is necessary. The complex cloud distributions contained within this study defy simple interpretations that have existed previously and a greater understanding is required before applying parameterizations in climate models. Moreover, the work that was done here seems to support the theory of the discrepancy in cloud model feedback being among low clouds. This is evidenced by the differences between the regions for ISCCP-defined cloud bins that have similar names, but different distributions as a function of height, e.g., stratocumulus, cumulus. The current suite of GCMs shows their largest uncertainty in climate feedback due to the clouds and Soden and Vecchi (2011) were able to show that most of the uncertainty is realized in the predicted occurrence of low-level clouds. Furthermore, Soden and Vecchi (2011) show that the feedback attributed to the low clouds is likely to be positive, i.e., the models in general tended to under-produce low-clouds in a changing climate and thus would

facilitate more warming. The intermodel disparity in GCMs that employ such parameterizations as provided from ISCCP-named bins could be, at least in part, according to this study be due to the ambiguous nature of these bins. It is worthwhile to note, however, that ISCCP-defined bins can retain some utility as long as they are understood to be a consequence of the radiative properties of the layer rather than representative of a physical cloud top.

Additionally, it is incorrect to assume that ISCCP cloud bins contain similar cloud distributions in different regions of the planet based on this limited analysis of the A-Train data. While the upper tropospheric types appear to be similar to one another in the East and West Pacific study regions, the middle and lower tropospheric types are significantly different in their vertical distributions of cloud layers, as alluded to in the results section. The West Pacific study region, for instance contains significantly more cirrus in the middle and lower tropospheric bins than is found in the East Pacific study region. This finding is not surprising because the ISCCP types and bins derived from them are really descriptive of column radiative properties and similarities in P_{top} and τ can be arrived at by any number of combinations of cloud location and microphysical properties. Others have found this as well. Chen and Del Genio (2009), for instance, show a disparity in the cloud occurrence statistics derived from millimeter radar at the Manus and Nauru ARM sites for a given ISCCP regime. This finding, while requiring additional study to quantify, implies that global regimes derived from the ISCCP P_{top}-τ statistics will not necessarily have the same clouds from region to region and from time to time even though they appear similar in the thermal IR and visible reflectance data.

REFERENCES

Bony, S., et al., 2006: How well do we understand and evaluate climate change feedback processes? *J. of Climate*, **19**, 3445–2461, doi:10.1175/JCLI3819.1.

Chen, Y. and A. Del Genio, 2009: Evaluation of tropical cloud regimes in observations and a general circulation model. *Climate Dynamics*, **32**, 355-369, DOI 10.1007/s00382-008-0386-6

Del Genio, A., A. Wolf and M. Yao, 2005: Evaluation of Regional Cloud Feedbacks Using Single-column Models. *J. Geophysical Res.*, **110**, D15S13, doi:10.1029/2004JD005011.

Dufrense, J. and S. Bony, 2008: An Assessment of the Primary Sources of Spread of Global Warming Estimates from Coupled Atmosphere–Ocean Models. *J. of Climate*, **21**, 5135-5144.

Hartmann, D.L., L.A. Moy and Q. Fu, 2001: Tropical Convection and the Energy Balance at the Top of the Atmosphere. *J. of Climate*, **14**, 4495–4511.

Iga, Shin-Ichi, T. Hirogumi, Y. Tsushmia, and S. Masaki, 2011: Sensitivity of Hadley circulation to physical parameters and resolution through changing upper-tropospheric ice clouds using a global cloud system resolving model. *J. of Climate*, **24**, DOI: 10.1175/2010JCLI13472.1, 2666-79

Im, E., S. L. Durden, and C. Wu, 2006: Cloud Profiling Radar for the CloudSat mission, IEEE Aerosp. *Electron. Syst. Mag.*, **20**, 15–18, doi:10.1109/MAES.2005.1581095.

Jakob, C. and G. Tselioudis, 2003: Objective identification of cloud regimes in the Tropical Western Pacific. *Geophysical Res. Letters,* **30**, 2082, doi:10.1029/2003GL018367.

Kiehl, J., 1994: On the Observed Near Cancellation between Longwave and Shortwave Cloud Forcing in Tropical Regions. *J. of Climate*, **7**, 559-565

Klein, S.A. and C. Jakob,1999: Validation and Sensitivities of Frontal Clouds Simulated by the ECMWF Model. *Monthly Weather Review*, **127**, 2514-2533.

Mace, G. G., et al., 2006: Cloud radiative heating at the ARM Climate Research Facility: Part 1. Technique, validation, and comparison to satellite-derived diagnostic quantities. *J. Geophys. Res.*, **111**, D11S90, doi:10.1029/2005JD005921.

Mace, G. G., Q. Zhang, M. Vaughan, R. Marchand, G. Stephens, C. Trepte, and D. Winker, 2009: A description of hydrometeor layer occurrence statistics derived from the first year of merged CloudSat and CALIPSO data, *J. Geophys. Res.*, **114**, D00A26, doi:10.1029/2007JD009755.

Mace, G. G., et al., 2010: Critical Evaluation of the ISCCP Simulator Using Ground-Based Remote Sensing Data. *J. of Climate*, **24**, 1598-1612, doi: 10.1175/2010JCLI3517.1

Partain, P., 2004: CloudSat ECMWF-AUX Auxiliary Data Process Description and Interface Control Document, Coop. Inst. For Res. In the Atmos., Colorado State Univ., Fort Collins.

Polonsky, I. N., L. C. Labonnote, and S. Cooper, 2008: Level 2 cloud optical depth product process description and interface control document, Coop. Inst. For Res. In the Atmos., Colorado State Univ., Fort Collins.

Rossow, W. and R.A. Schiffer, 1991: ISCCP Cloud Data Products. *Bull. Amer. Meteor. Soc.*, **72**, DOI: 10.1175/1520-0477(1991)072<0002:ICDP>2.0.CO;2

Rossow, W. and R.A. Schiffer, 1999: Advances in understanding clouds from ISCCP, *Bull. Am. Meteorol. Soc.*, **80**, 2261–2288, doi:10.1175/1520-0477(1999)080<2261:AIUCFI>2.0.CO;2.

Rossow, W. and Y. Zhang, 1995: Calculation of surface and top of atmosphere radiative fluxes from physical quantities based on ISCCP data sets 2. Validation and first results. *J. Geophysical Res.*, **100**, 1167-1197, doi:10.1029/94JD02746

Schwartz, C. and G.G. Mace, 2010: Co-occurrence statistics of tropical tropopause layer cirrus with lower cloud layers as derived from CloudSat and CALIPSO data. *J. Geophys. Res.*, **115**, doi:10.1029/2009JD012778

Soden, B. and G. Vecchi, 2011: The vertical distribution of cloud feedback in coupled ocean-atmosphere models. *Geophys. Res. Lett*., **38**, doi:10.1029/2011GL047632

Stephens, G. L., 2005: Cloud feedbacks in the climate system: A critical review. *J. Atmos. Sci.*, **18**, 237–273.

Wang J. and W. Rossow, 1998 Effects of Cloud Vertical Structure on Atmospheric Circulation in the GISS GCM. *J. of Climate*. **11**, 3010-3029.

Webb, M.,C. Senior, S. Bony, and J.-J. Morcrette, 2001: Combining ERBE and ISCCP data to assess clouds in the Hadley Centre, ECMWF and LMD atmospheric climate models. *Climate Dyn.*, **17**, 905–922.

Williams, K. D., and G. Tselioudis, 2007: GCM intercomparison of global cloud regimes: Present-day evaluation and climate change response. *Clim. Dyn.*, **29**, 231–250, doi:10.1007/s00382-007-0232-2.

Williams, K.D. and M.J. Webb, 2009: A Quantitative Performance Assessment of Cloud Regimes in Climate Models. *Climate Dynamics*, **33**, 141-157.

Winker, D. M., B. H. Hunt, and M. J. McGill, 2007: Initial performance assessment of CALIOP, *Geophys. Res. Lett.*, **34**, L19803, doi:10.1029/ 2007GL030135.

Zhang, M. H., et al., 2005: Comparing Clouds and their Seasonal Variations in 10 Atmospheric General Circulation Models with Satellite Measurements. *J. Geophysical Res.*, **110**, D15S02, doi:10.1029/2004JD005021.